Glacier thickness, thermal regime, and subjective uncertainty from ground-penetrating radar of 25 Svalbard glaciers

Journal:	*Journal of Glaciology*
Manuscript ID	JOG-2025-0183.R1
Manuscript Type:	Article
Date Submitted by the Author:	25-Jun-2026
Complete List of Authors:	Schytt Mannerfelt, Erik; University of Oslo Faculty of Mathematics and Natural Sciences, Department of Geosciences; University Centre in Svalbard, Arctic Geology Enzenhofer, Ursula; Norwegian University of Science and Technology, Department of Geography and Social Anthropology; University Centre in Svalbard, Arctic Geology Innanen, Satu; University of Oslo Faculty of Mathematics and Natural Sciences, Department of Geosciences Aberhalden, Jogscha; Western Norway University of Applied Sciences, Department of Civil Engineering and Environmental Sciences Ploeg, Karlijn; University of Bergen Faculty of Mathematics and Natural Sciences, Department of Earth Science; Bjerknes Centre for Climate Research Brunner, Johannes; University of Oslo Faculty of Mathematics and Natural Sciences, Department of Geosciences Gillespie, Mette; Western Norway University of Applied Sciences, Department of Civil Engineering and Environmental Sciences; VIA University College Kleber, Gabrielle; UiT The Arctic University of Norway Faculty of Science and Technology, Department of Geoscience Kolar, Jonathan; University of Lausanne Institute of Earth Sciences Moholdt, Geir; Norsk Polarinstitutt, Solem, Solveig; Norwegian Water Resources and Energy Directorate,

	Department of Hydrology hodson, andrew; University Centre in Svalbard, Arctic Geology
Keywords:	Ground-penetrating radar, Ice thickness measurements, Ice temperature, Glacier geophysics
Abstract:	Glacier thickness and thermal regime control glacier dynamics and long-term evolution, but observations are sparse at regional scales. Both can be measured using ground-penetrating radar (GPR), which requires manual or automated interpretation. Interpretation often depends on more than signal waveform analysis alone, and this subjectivity has not been thoroughly quantified before. We present 699 km of ground-based GPR data from 25 glaciers in Svalbard, after crowd-sourcing glacier bed and cold-temperate transition surface (CTS) interpretations from 41 contributors. We find that subjective uncertainty is usually smaller than instrument-related uncertainties for the glacier bed, though notable exceptions exist from off-nadir reflections or occlusion by temperate ice. CTS interpretations have higher spreads and show qualitative disagreement in the required amount of scatter to be considered as temperate ice. Our thermal regime consensus estimates reveal a wide diversity in temperate ice extent and distribution between glaciers, as well as insights into the thermal structure of glaciers with surge-related histories. Our thickness consensus agrees with previous measurements, and we show that thickness inversion model performance varies with thermal regime. All data are available to enable novel applications and automated bed/CTS detection methods that acknowledge interpretation uncertainty.

Glacier thickness, thermal regime, and subjective uncertainty from ground-penetrating radar of 25 Svalbard glaciers

Erik Schytt MANNERFELT,[1,2] Ursula ENZENHOFER,[2,3] Satu INNANEN,[1] Jogscha M. ABDERHALDEN,[4] Karlijn PLOEG,[5] Johannes BRUNNER,[1] Mette Kusk GILLESPIE[4,6], Gabrielle E. KLEBER,[7] Jonathan KOLAR,[8] Geir MOHOLDT,[9] Solveig SOLEM[10] and Andrew J. HODSON[2]

[1]*Department of Geosciences, University of Oslo, Oslo, Norway*

[2]*Arctic Geology, The University Centre in Svalbard, Longyearbyen, Norway*

[3]*Department of Geography and Social Anthropology, NTNU, Trondheim, Norway*

[4]*Department of Civil Engineering and Environmental Sciences, Western Norway University of Applied Sciences, Sogndal, Norway*

[5]*Department of Earth Science, University of Bergen and Bjerknes Centre for Climate Research, Bergen, Norway*

[6]*VIA University College, Nørre Nissum, Denmark*

[7]*Department of Geoscience, UiT the Arctic University of Norway, Tromsø, Norway*

[8]*Institute of Earth Sciences (ISTE), University of Lausanne, Lausanne, Switzerland*

[9]*Glaciology and Geology Section, Norwegian Polar Institute, Fram Centre, Tromsø, Norway*

[10]*Department of Hydrology, Norwegian Water Resources and Energy Directorate (NVE), Oslo, Norway*

Correspondence: <e.s.mannerfelt@geo.uio.no>

25th June 2026

ABSTRACT. Glacier thickness and thermal regime control glacier dynamics and long-term evolution, but observations are sparse at regional scales. Both can be measured using ground-penetrating radar (GPR), which requires manual or automated interpretation. Interpretation often depends on more than signal waveform analysis alone, and this subjectivity has not been thoroughly quantified before. We present 699 km of ground-based GPR data from 25 glaciers in Svalbard, after crowd-sourcing glacier bed and cold-temperate transition surface (CTS) interpretations from 41 contributors. We find that subjective uncertainty is usually smaller than instrument-related uncertainties for the glacier bed, though notable exceptions exist from off-nadir reflections or occlusion by temperate ice. CTS interpretations have higher spreads and show qualitative disagreement in the required amount of scatter to be considered as temperate ice. Our thermal regime consensus estimates reveal a wide diversity in temperate ice extent and distribution between glaciers, as well as insights into the thermal structure of glaciers with surge-related histories. Our thickness consensus agrees with previous measurements, and we show that thickness inversion model performance varies with thermal regime. All data are available to enable novel applications and automated bed/CTS detection methods that acknowledge interpretation uncertainty.

1 INTRODUCTION

Glacier ice thickness and thermal regime exert fundamental controls on glacier dynamics and long-term evolution. Ice thickness is a primary control on glacier geometry, volume and driving stress, and therefore influences deformation, while the thermal regime strongly affects ice viscosity, basal sliding potential and subglacial hydrology (Cuffey and Paterson, 2010). Despite their importance, both variables remain poorly constrained at scale because they require direct in situ measurements. These measurements can be obtained using geophysical methods, such as ground-penetrating radar (GPR), which is the most common method for measuring subsurface properties of glaciers (Macheret and Zhuravlev, 1982; Dowdeswell and others, 1984; Plewes and Hubbard, 2001; Schlegel and others, 2022). The Glacier Thickness Database (GlaThiDa)

(Gärtner-Roer and others, 2014; Welty and others, 2020) and the global englacial temperature database (glenglat) (Jacquemart and others, 2025) are community databases facilitating the availability of glacier thickness and englacial temperature data. With growing datasets and more frequent usage through these databases, assessing uncertainty becomes critical. In glacier radargrams, the glacier bed is commonly identified as a sparse or fully continuous subsurface reflector, caused by the strong dielectric contrast between ice and the underlying substrate. Clean bedrock, dry sediment, wet sediment or water, all contrast differently and the glacier bed may therefore reflect differently across or within glaciers (Gades and others, 2000; Copland and Sharp, 2001; Wilson and others, 2014). Therefore, delineating the glacier bed may vary in difficulty depending on the location, and there may be a variable degree of subjectivity involved. While the uncertainties associated with the GPR instrument and positioning data are well characterised by Lapazaran and others (2016), the uncertainty of subjective interpretations remains largely unquantified. To ensure transparency when reporting GPR data uncertainty, it is necessary to evaluate the magnitude of this component.

The archipelago of Svalbard has more ice cover than exposed land (57%, 1583 glaciers by count; Nuth and others, 2013), yet only 213 of its glaciers and ice caps have measurements in GlaThiDa as of December 2025. Glacier thickness inversion modelling, which is increasingly used for estimating ice thickness in Svalbard and beyond, uses glacier physics and surface expressions to infer the glacier thickness, thereby enabling estimates in regions without direct measurements (Fürst and others, 2018; Millan and others, 2022; van Pelt and Frank, 2025; Maffezzoli and others, 2025; Steidl and others, 2025). Inversion models are often calibrated with GlaThiDa data, and consequently, their overall performance depends on the abundance and quality of thickness measurements. Obtaining more measurements and improving inversion models is highly relevant, as model estimates of global glacier volume — and thus sea-level contribution potential — currently disagree by about 25% (Farinotti and others, 2019).

Thermal conditions within Svalbard glaciers are not yet well constrained. Existing measurements show high variability among glaciers — for example, temperate ice fractions vary from 1 to 74% in 16 glaciers near the west coast of Spitsbergen (Macheret and others, 2019) — and substantial differences exist between neighbouring glaciers in both the southwest (Jania and others, 1996; Ødegård and others, 1997; Grabiec, 2017) and northwest (Björnsson and others, 1996; Karušs and others, 2022). The cold-temperate transition surface (CTS), marks the transition between dry (cold) and water-saturated (temperate) ice and serves as a proxy for englacial thermal structure. This "zero water content isoline" has been shown to agree well

with the zero degree isotherm from borehole measurements (Björnsson and others, 1996; Ødegård and others, 1997), though water content seasonality near glacier termini could complicate the relationship in some cases (Irvine-Fynn and others, 2006). The CTS is typically mapped from radargrams as the upper boundary of diffuse reflectors, interpreted as water pockets. This visual threshold is subjective to the point where even repeat mappings by the same person may vary (Gusmeroli and others, 2012), and quantifying its variability further would be a step to improving its definition.

Svalbard has an unusually high frequency of unstable glacier behaviour, most commonly expressed as glacier surges (Sevestre and Benn, 2015; Kääb and others, 2023; Guillet and others, 2025). A surging glacier manifests an internal imbalance through a substantial (usually 10–1000 times) velocity increase for a number of years (e.g. Guillet and others, 2025), before stagnating and experiencing a prolonged period of quiescent (slow) activity (Meier and Post, 1969). Surging has been observed in about a third of all glaciers in Svalbard, yet up to 90% have been inferred to have this behaviour by indirect evidence (Hagen and others, 1993; Harcourt and others, 2025). Thermal regulation is one current theory for explaining surging (Fowler and others, 2001; Sevestre and others, 2015). Therefore, while the exploration of surge dynamics is not a primary objective of this study, a glacier's surge history is important to consider when interpreting and discussing a glacier's thermal regime.

The aim of this study is to 1) provide, analyse and discuss new data on Svalbard glacier thickness and thermal regime, and 2) quantify interpretation uncertainty and compare it to instrument-related magnitudes. We use these results to evaluate when manual GPR interpretation is robust, when it becomes ambiguous, and how such uncertainty should inform future radar interpretation studies and developments in automation. We present new GPR data from 25 Svalbard glaciers, providing the largest surface-coupled glacier thickness measurement addition to date to GlaThiDa, and the first CTS data contribution to glenglat. We compare thickness inversion model performances, and finally discuss thermal regime patterns in relation to surging, and future data-sharing initiatives.

2 DATA AND METHODS

2.1 Data acquisition

We present new GPR data from 25 glaciers in Svalbard, collected through numerous field campaigns between 2019 and 2025 constituting 699 km of total profile length (Fig. 1, Table 1). The processing steps are visualised in Figure 2. All data were collected between January and May, with GPR antennas towed in

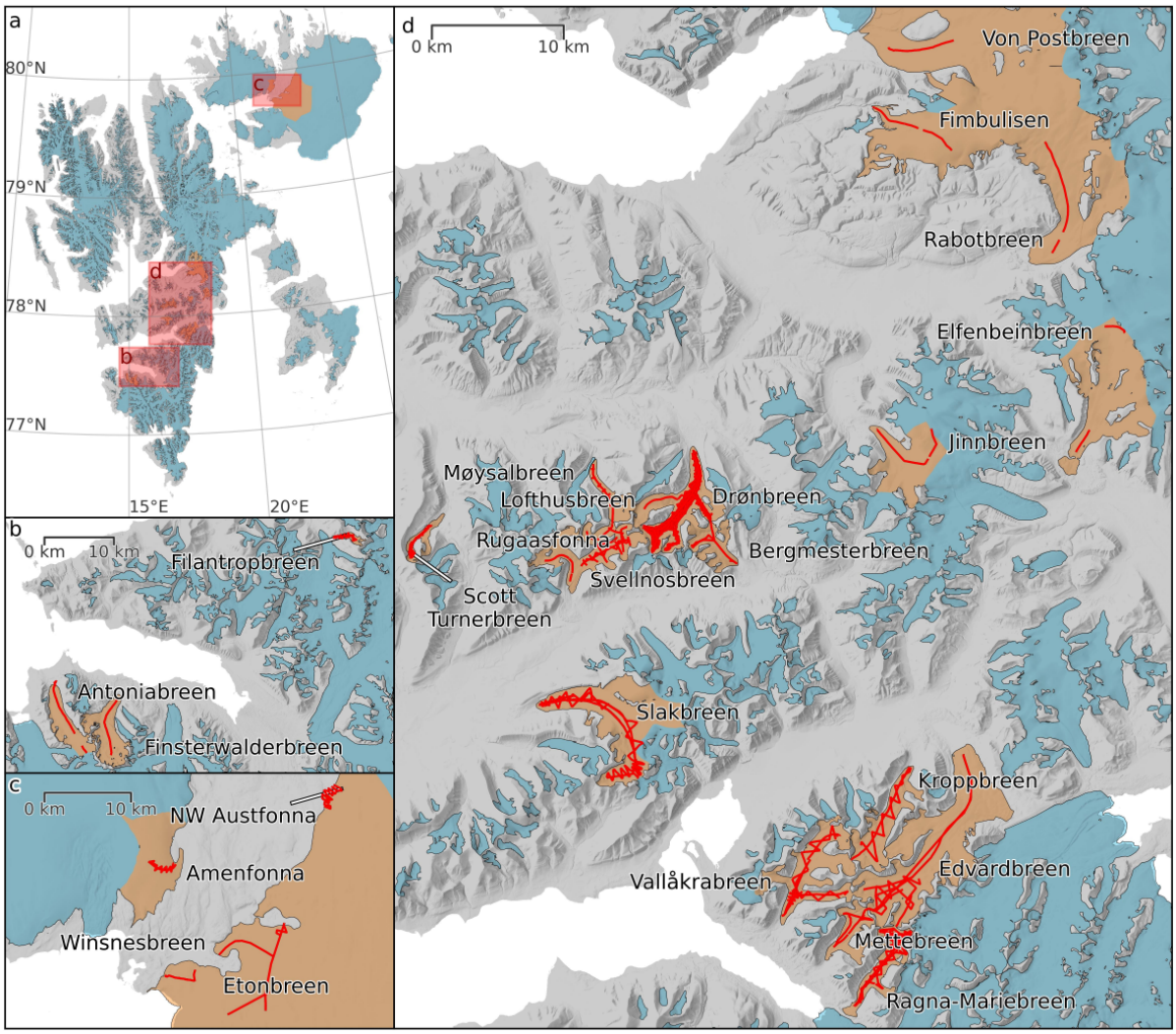

Figure 1. Location of the surveyed glaciers in Svalbard (**a**), showing insets for **b:** glaciers in Nathorst Land, **c:** in Nordaustlandet, and **d:** in Nordenskiöld Land and Heer Land. The survey tracks are shown in red lines. Surveyed glaciers are highlighted in orange and all other glaciers are shown in blue. Hillshade basemap is from the Norwegian Polar Institute (2014b), and glacier outlines are from Nuth and others (2013).

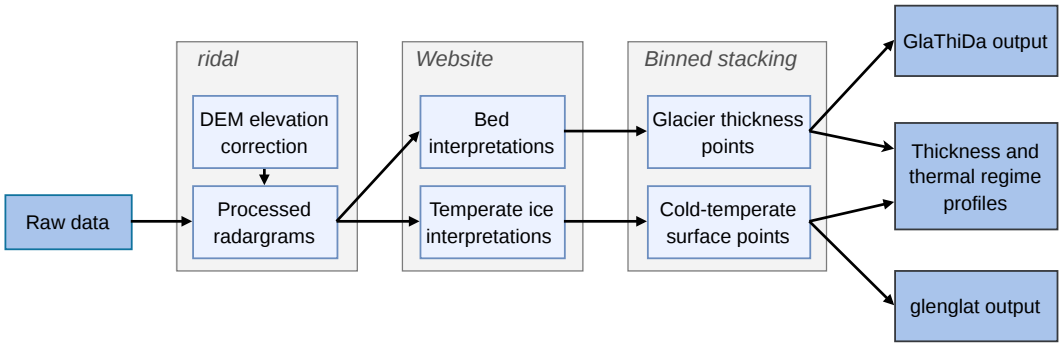

Figure 2. Processing workflow summarising the methodology of the study.

a co-linear Rx-Tx configuration behind snowmobiles at a driving speed between 10 and 15 km/h. The radar systems were various Malå ProEx units and rough terrain antennas with centre frequencies of 25 MHz (40 profiles), 50 MHz (4 profiles) and 100 MHz (94 profiles). The majority of surveys were collected with a trace interval of 0.2 s, leading to a trace spacing of roughly 0.5–0.8 m per trace. Positioning was acquired with different real-time fix GNSS receivers (most often GlobalSat BU-353S4 units) with a limited horizontal positioning accuracy (∼10 m). The number of samples per trace varied between 1300 and 2024 at sampling frequencies of 8-21× the antenna centre frequency. Exact acquisition parameters for each radargram are available in the data publication. Due to varying survey objectives and team composition, acquisition strategies ranged from simple centreline profiles to zig-zag patterns, ice flow-perpendicular transects, and localised high-resolution surveys (Fig. 1).

2.2 Elevation coordinate correction

Having high-accuracy information on the elevation of our radargrams is not necessary for the primary objectives of this study, but we still refine this information to improve profile plots and future data use. We account for the poor vertical accuracy of the GNSS receivers using ArcticDEM data for elevation coordinate correction (Porter and others, 2018). For each glacier and survey year, we pick the closest year (within two years) to the acquisition date that has good ArcticDEM coverage and compute an annual co-registered median elevation product for the glacier. We use the Svalbard S0 Digital Elevation Model (DEM) (Norwegian Polar Institute, 2014b) as an accurate (reported 1–5 m) but outdated (by 10–13 years) reference for horizontal and vertical (orthometric) co-registration over stable terrain. As a stable terrain mask, we use areas outside the geometric union of glacier outlines from 1936 (Geyman and others, 2022)

Table 1. Summary of key parameters of the studied glaciers, ordered from north to south (cf. Fig. 1). The glacier area and elevation ranges are from Nuth and others (2013). A surge history with "No date" represents indications but no direct observation of surging in the last one or two centuries. Dashes represent no known indication or observation.

Glacier	Area (km²)	Elevation range (m a.s.l.)	GPR profile length (km)	Last surge
NW Austfonna	112	239–739	12	-
Amenfonna	56	41–556	23	-
Winsnesbreen	243	48–797	22	-
Etonbreen	641	0–1000	41	2023[1]
Von Postbreen	168	19–1046	6	1870[2]
Fimbulisen	35	248–756	5	-
Rabotbreen	70	61–828	9	-
Elfenbeinbreen	41	48–668	2	1903[2]
Jinnbreen	20	160–844	6	No date[2]
Møysalbreen	5	285–939	20	1925[2]
Lofthusbreen	21	208–935	2	1896[3]
Drønbreen	21	208–935	209	1896[3]
Scott Turnerbreen	3	241–961	11	1914[3]
Bergmesterbreen	8	240–894	9	No date[2]
Rugaasfonna	18	168–958	81	No date[2]
Svellnosbreen	18	168–958	12	No date[2]
Slakbreen	36	162–983	68	-
Kroppbreen	15	56–801	19	2000s[4]
Edvardbreen	58	31–814	50	∼2025[1]
Vallåkrabreen	22	69–847	26	2022[1]
Mettebreen	8	135–839	9	No date[2]
Ragna-Mariebreen	10	58–847	53	No date[2]
Filantropbreen	4	236–998	9	No date[2]
Antoniabreen	27	49–876	11	No date[2]
Finsterwalderbreen	34	30–996	9	1914[2]

[1] Mannerfelt and others (2025), [2] Harcourt and others (2025), [3] Mannerfelt and others (2024), [4] Sund and others (2009).

and moraines, braided rivers, lakes and ocean (Norwegian Polar Institute, 2014a). We then use the Iterative Closest Point and Nuth and Kääb (2011) sub-pixel adjustment co-registration pipeline implemented in the xdem Python package (xdem contributors, 2021), following Mannerfelt and others (2022).

2.3 GPR processing

We autonomously process the GPR data by applying a pre-set sequence of filters in the software *Ridal* version 0.4.7 (`https://github.com/erikmannerfelt/ridal`). The software implements a range of commonly used filters for radar processing, and is specifically made for performant batch processing. The processing chain consists of these filters in succession: empty trace removal, global time-zero correction, Rx-Tx antenna-separation correction, Butterworth bandpass (program-default settings), dewow, exponential gain, signed log10 magnitude conversion, and a time-to-depth conversion using a radar wave velocity of 0.168 m ns^{-1} (e.g. Bælum and Benn, 2011; Navarro and others, 2015; Lapazaran and others, 2016). We do not apply migration (see Supplementary Text). A consistent gain is applied across radargrams for the same antenna frequency. For each radargram, we first determine an optimal exponential gain value by automatically estimating it from the attenuated reflection strength with depth, and then apply the per-frequency median gain to each radargram. Thus, the radargrams are generally comparable in reflection strength for the same frequency, but limitations of this general treatment are discussed later.

2.4 Multi-operator-based interpretation

To assess subjective uncertainty in GPR data interpretation and to gain a robust consensus estimate, we crowd-sourced the interpretation of all radargrams by inviting contributors from the glaciology community. Contributions were accepted from individuals with self-reported experience in glacier radar. In total, 41 people from 30 different institutions and 12 countries contributed in the experiment. We received 1498 radargram interpretation submissions (average 37 per person) with 10.9 contributions per radargram on average and up to 24 contributions in individual cases.

Radargrams were available on a dedicated website created for this study (archival version available at `https://erikmannerfelt.github.io/svalbard_radar_web`). We provided an instruction set for the interpretations, showing conceptual examples and taking care in weighing instruction clarity against over-dictating how interpretation should be made. Each contributor's non-identifying username was assigned by one contact author. The other authors who developed the consensus-estimation functionality had no

access to the identity-username mapping to avoid partiality. The contribution interface consisted of a page with information about radar acquisition parameters, a satellite map showing the location track, and the radargram itself with a choice between two options for how the values of the radargram are displayed: absolute or signed value scaling. The contributor added polylines on the radargram, choosing from four different classes: "Glacier bed", "Temperate ice" (described as its upper boundary in the instruction set), "Glacier bed (no temperate ice)", and "Glacier bed not visible" (Fig. 3).

2.5 Consensus estimation

For each radargram, we calculate a consensus estimate for all contributors' line interpretations at a horizontal spacing of 5 m per vertex. Specifically, we extract one line for ice thickness and one for the CTS, along with the upper and lower (25–75 percentiles) for both. The bounds are obtained from a quantile operation for each 5 m sample vertex, and the median (0.5 quantile) serves as the primary estimate. For ice thickness, we use the two glacier bed classes ("Glacier bed" and "Glacier bed (no temperate ice)"). For the CTS, we use the "Glacier bed (no temperate ice)" as a zero value, and the "Temperate ice" class for non-zero values. All traces that have more "Glacier bed not visible" than glacier bed observations are removed completely (Fig. 3e,f).

2.6 Uncertainty estimation

To assess point-wise ice thickness and CTS depth uncertainty (ϵ_H) in our data, we use a formulation that closely resembles that of Lapazaran and others (2016), except we include a term for subjectivity in their uncertainty formulation:

$$\epsilon_H = \sqrt{\epsilon^2_{H_{gpr}} + \epsilon^2_{H_{contributor}} + \epsilon^2_{H_{xy}}}, \tag{1}$$

where $\epsilon_{H_{gpr}}$ is the GPR-related uncertainty, $\epsilon_{H_{contributor}}$ is the contributor spread in our measurements, and $\epsilon_{H_{xy}}$ is the GNSS-related positional uncertainty, translated to vertical uncertainty based on the bed slope. For other required assumptions in the formulation (see Lapazaran and others, 2016), we consider a medium velocity uncertainty of 2% (Jania and others, 2005; Bradford and others, 2009), a GNSS-to-GPR timing uncertainty of 1 s (taken from the GNSS sampling frequency), and a GNSS positioning uncertainty of 10 m. We use the Normalised Median Absolute Deviation (NMAD; 1.4826× the standard deviation for a normal distribution) as a robust spread estimator (Leys and others, 2013).

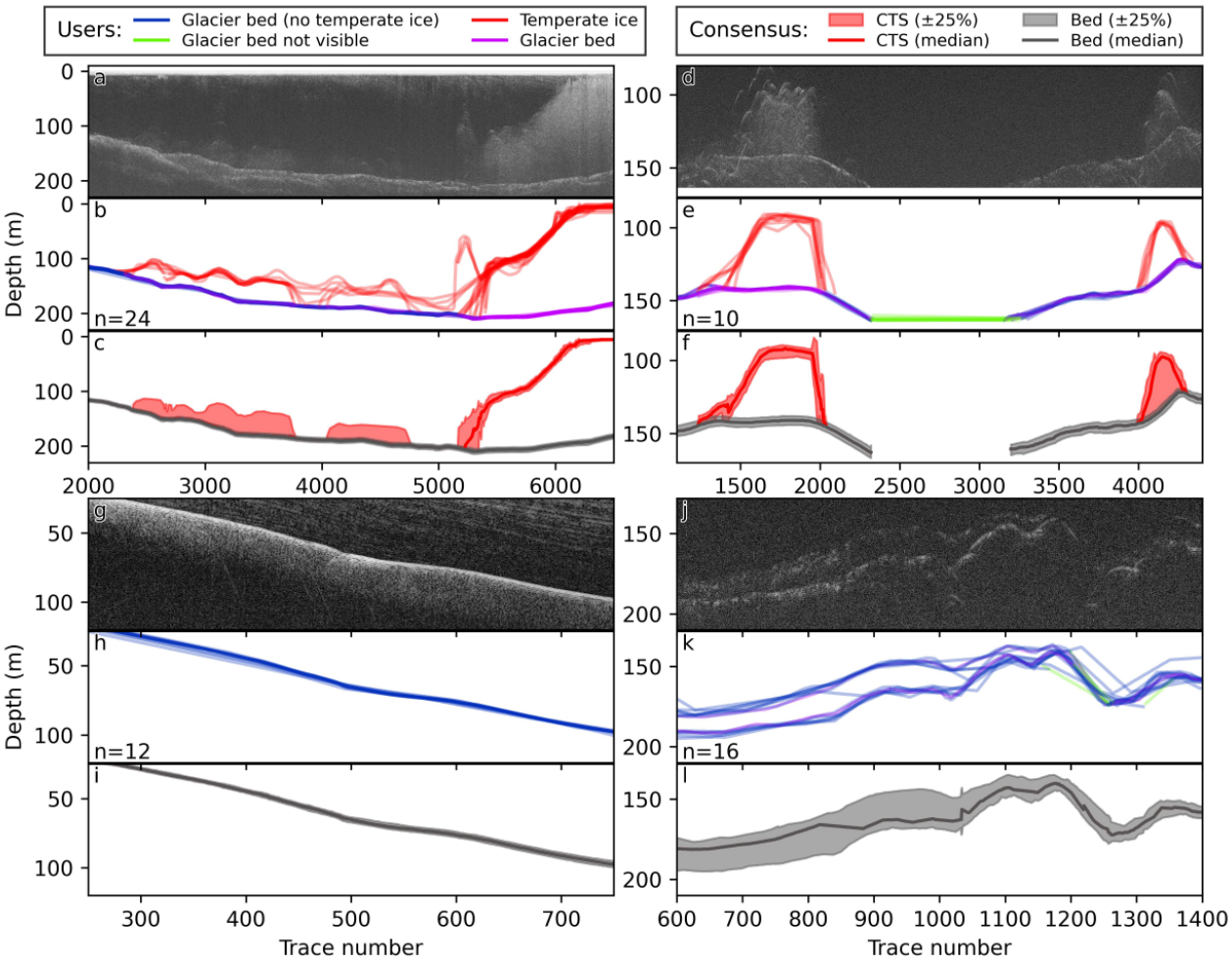

Figure 3. Examples of individual radargram interpretations and the final consensus estimates. **a:** Radargram from Ragna-Mariebreen (100 MHz) showing glacier bed and temperate ice reflections. Low-magnitude parts are black and high-magnitude parts are white. **b:** All subsequent interpretations by contributors (n is the number of contributors). **c:** Consensus thickness and temperate ice estimates based on every contributor's contribution. **d, e, f:** Example from Drønbreen (100 MHz), e.g. showing a consensus of a missing glacier bed. **g, h, i:** Example of an easily interpretable glacier bed without temperate ice from the ice cap Amenfonna (25 MHz). **j, k, l**: Example at Winsnesbreen (25 MHz) of two potential glacier bed interpretations accounted for in the consensus spread.

Table 2. Previous surveys in the GlaThiDa (December 2025 version) which are used for comparison to our data. The year and reference are reproduced exactly as stated in the database.

Glacier	Year	Platform	Reference
NW Austfonna	2008	Ground	Vasilenko and others (2009)
Winsnesbreen & Etonbreen	1983	Airborne	Dowdeswell and others (1986)
	2008	Ground	Vasilenko and others (2009)
	2017	Airborne	Paden and others (2010)
Elfenbeinbreen	2014	Ground	Navarro and others (2015)
Slakbreen	1980	Airborne	Dowdeswell and others (1984)
	1989	Ground	Hamran and Aarholt (1993)
	2000–2002	Ground	Schuler and Melvold (2004)
	2021	Ground	Borisik and others (2022)
Kroppbreen	1986	Airborne	Dowdeswell and others (1984)
Edvardbreen	1986	Airborne	Dowdeswell and others (1984)
Vallåkrabreen	1986	Airborne	Dowdeswell and others (1984)
Ragna-Mariebreen	1986	Airborne	Dowdeswell and others (1984)
Finsterwalderbreen	1980	Airborne	Dowdeswell and others (1984)

2.7 Data comparisons

As a measure for internal data consistency between surveys, antennas and picking consensus, we perform a crossover analysis by comparing the ice thickness and CTS depth of all intersecting points across profiles. We also perform a crossover analysis between our thickness data and previously existing GlaThiDa entries, to discuss interpretation consistency and deviations from archival entries. Previous surveys that intersect with ours in the GlaThiDa are summarized in Table 2. Finally, we compare our thickness measurements to three publicly available thickness inversion products: Fürst and others (2018, version 1.1), Millan and others (2022) and van Pelt and Frank (2025).

When comparing thickness data of different acquisition dates, we apply a simple temporal thickness correction to make them more comparable. Specifically, we sample the January 2000 to December 2019 elevation change rate from Hugonnet and others (2021) and multiply this rate by the year difference to a standard year, here chosen to be 2015. We choose the 20-year average rate instead of the available 5- or 10-year averages due to the lower uncertainty of the longer time-period. For archival data comparisons, we instead use elevation change rates from 1936–2010 by Geyman and others (2022) as a more representative

dataset for 20th century mass balance conditions. For years in the overlapping range of 2000–2010, we linearly blend the two products to avoid boundary effects. We also apply this correction to thickness comparisons from inversion models. For Fürst and others (2018), we consider their stated representative date as 2010. For Millan and others (2022) and van Pelt and Frank (2025), with stated date ranges of 2017–2018 and 2010–2015, respectively, we use the average of each range. This also influenced the arbitrary choice of using 2015 as the standard year because it is an approximate average, although all data (including ours) are corrected so the exact year choice should not have a measurable effect.

3 RESULTS

3.1 Interpretation and total uncertainty

Figure 3 shows examples of glacier bed and CTS interpretations from radargrams and the final consensus estimates. Glacier bed interpretations are generally consistent, resulting in a low spread (Fig. 3c,f,i). In some cases, however, the glacier bed is ambiguous due to multiple possible bed reflections (Fig. 3j), leading to systematic disagreements between the bed interpretations. Traces with more "Glacier bed not visible" entries than bed interpretations are excluded (Fig. 3f). In CTS interpretation, contributors tend to disagree on how much internal scattering is enough to interpret it as temperate ice or not. For example, Figure 3a-c shows a strong consensus after trace 5300, but there is large disagreement between traces 2200 and 5300: some use the "Glacier bed (no temperate ice)" class indicating no temperate ice above the bed (blue line), while others map the bed with the "Glacier bed" class (purple line) and interpret the scattering as temperate ice (red line). Areas like these with higher disagreement between the contributors are reflected in the consensus percentiles and subsequent uncertainty measures.

Across all radargrams, we use Equation 1 to calculate a median (±NMAD between radargrams) total thickness uncertainty of 3.0±1.2 m. For 25 MHz radargrams, the same total uncertainty is 3.6±1.4 m, and for 100 MHz, it is 2.8±1.0 m. The largest contributor is $\epsilon_{H_{GPR}}$ (the effect of antenna frequency and medium velocity uncertainty) of 2.5±1.2 m for all radargrams combined. This is clearly larger than the vertical component of the positioning uncertainty $\epsilon_{H_{xy}}$ of 0.6±0.6 m, and the consensus spread $\epsilon_{H_{contributor}}$ of 0.7±0.4 m. Similarly, the equivalent $\epsilon_{H_{contributor}}$ for CTS measurements is 6.2±4.3 m. Crossover differences (Fig. 4) reveal lower NMADs of 1.5 m for glacier thickness and 5.3 m for the CTS, hinting that our calculated uncertainties may be conservative (an overestimation). However, crossover differences only reveal internal consistency, not systematic biases, so this approach cannot be used to fully validate the accuracy of our

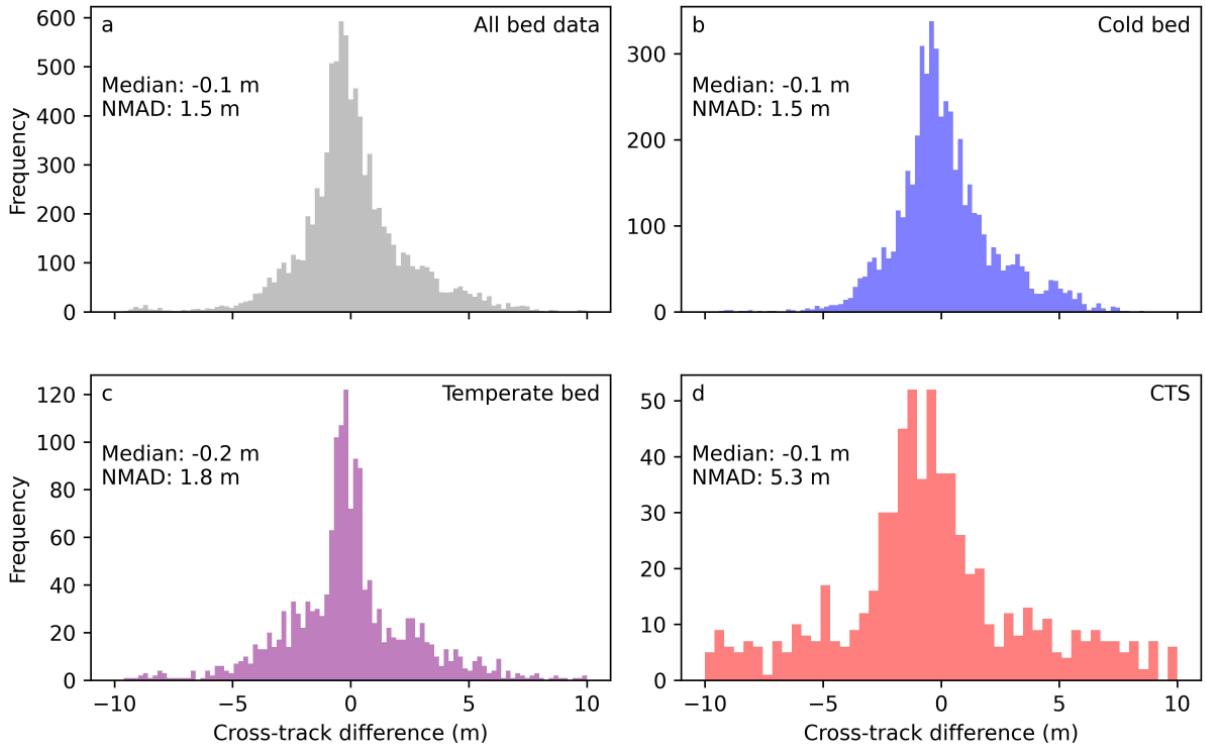

Figure 4. Crossover differences for all radargrams within the same year. **a:** differences for all data, **b:** differences on a cold bed (temperate ice absent), and **c:** differences on a temperate bed (temperate ice present). **d:** Crossover differences of the cold-temperate transition surface (CTS).

uncertainty assessment.

There is a small difference between both crossover differences and consensus spreads ($\epsilon_{H_{contributor}}$) for different antenna centre frequencies. For 25 MHz data, the crossover/contributor spread is 1.3/0.9 m, respectively, while for 100 MHz data, we find lower uncertainties of 1.2/0.6 m. This indicates that interpretations made on 100 MHz data have a slightly higher vertical accuracy than 25 MHz. When normalizing by the respective wavelength, however, 25 MHz data show an uncertainty of 20/14% of one wavelength, while 100 MHz data show uncertainties of 74/37%. This indicates that although 100 MHz data have a higher vertical resolution, they may be more ambiguous to interpret compared to 25 MHz data, which are easier to interpret with respect to their lower resolution. A visual comparison of this effect is shown in Figure S3.

3.2 CTS geometry

We observe a wide range of thermal regime configurations (Fig. 5). Profiles measured along centrelines show temperate ice fractions of 0–67%, and the average across the entire dataset is 16%. The most consistent

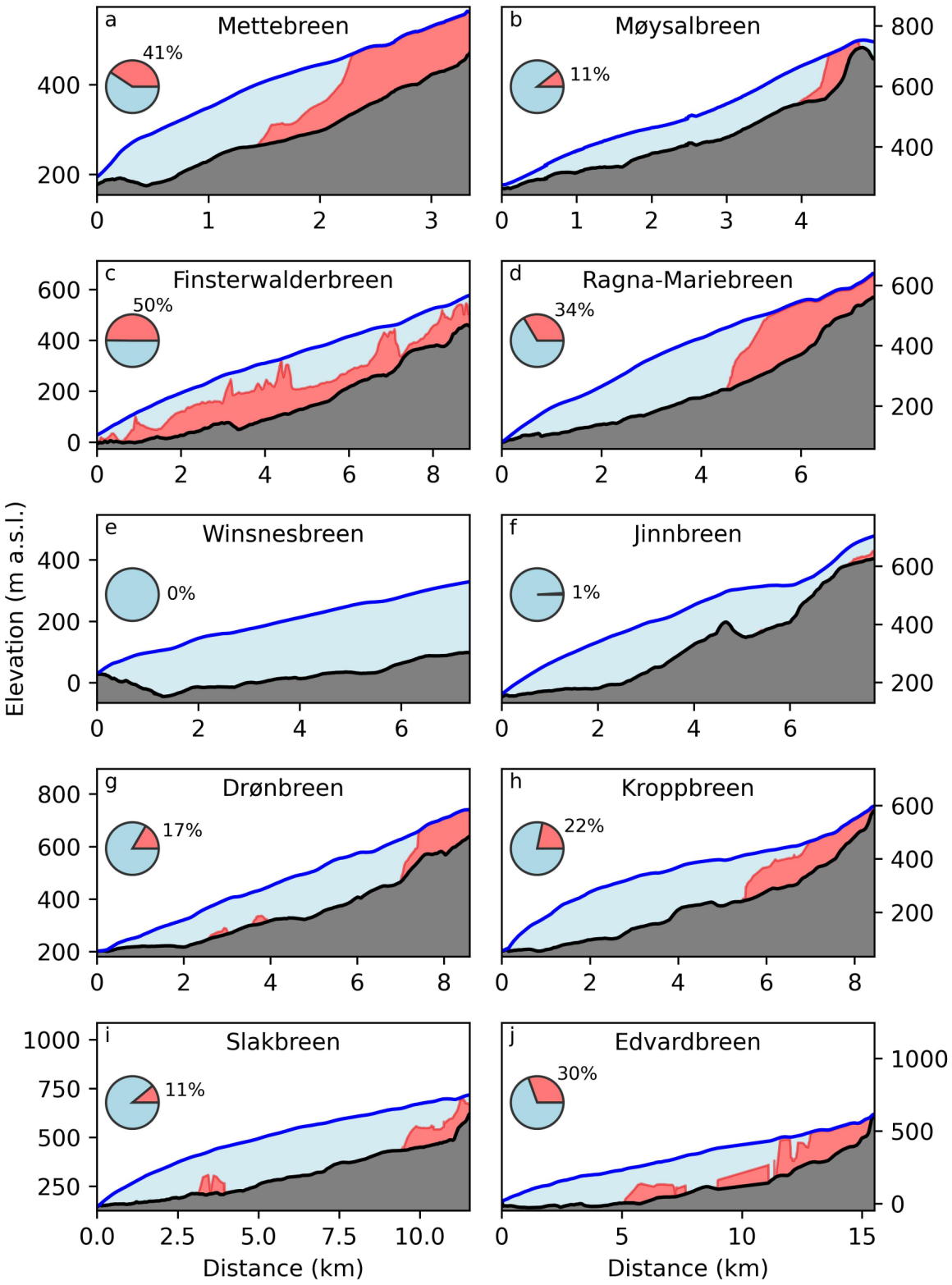

Figure 5. Glacier centreline profiles. Red areas represent the consensus median temperate ice estimate, and blue is equivalently cold ice. **a-b** have an 8× vertical exaggeration, and **c-j** have a 12× vertical exaggeration. The pie charts represent the fraction of temperate ice for each profile.

pattern is that temperate ice is more prevalent at higher elevations, where the CTS often connects to the surface, likely indicating active temperate ice production. In contrast, isolated patches of temperate ice occur in some locations without clear connections to the glaciers' active production zones (Drønbreen, Slakbreen, Edvardbreen; Fig. S6), and in others, we observe no temperate ice at all in the surveyed profiles (e.g. Winsnesbreen). Finally, some profiles reveal spikes of shallower CTS delineations, which may indicate temperate ice production downstream of the accumulation area through crevassing or other entryways (e.g. Finsterwalderbreen, Edvardbreen).

We calculate the steepness (thickness change over distance) of the thermal transition between cold glacier termini ($\leq$5% temperate ice in the column) and temperate accumulation areas ($\geq$95%), and find cases of notable steepness. At Ragna-Mariebreen, the transition occurs at an average thickness of 203 m over a distance of 800 m along the centreline, leading to a slope of 14°. Similarly, the equivalent transition slope at Drønbreen is 18° (137 m change over 415 m; cf. Fig. S6), and at Vallåkrabreen it is 34° (154 m change over 225 m). This contrasts to other glaciers that either have shallow transitions, such as Slakbreen (7°), Kroppbreen (6°) or Edvardbreen (4°), or have temperate ice throughout the glacier and thus have no transition zone at all (e.g. Finsterwalderbreen and Antoniabreen).

3.3 Comparison to earlier studies

Our new data agree with recently published GlaThiDa entries (after 2010), and differences in the comparison of older data likely reflect both nonlinear glacier thickness changes since the earlier surveys and the lower instrument precision typical of older studies (Fig. 6). A total least-squares fit for each period indicates proximity to a 1:1 relation to our estimates (0.96–1.07), and deviations are most likely from imperfections in the temporal thickness correction or instrument errors. We notice a progressively larger NMAD with age, being 3.7 m for data after 2010 but 23.1 m for data before 1990, where the latter is predominantly from airborne surveys. Temporally uncorrected comparisons can be seen in Figure S1.

3.4 Comparison to inversion products

We compare our newly collected glacier thickness data with modelled thickness inversion products (Fig. 7). In general, the models tend to reproduce similar values, with total least squares fits between 0.85 and 1.37 (1 is optimal). Among the models, Millan and others (2022) shows the lowest spread, with an NMAD of 40.0 m. The models show biases of -10.6 m to 3.6 m, with some further discrepancies, such as most

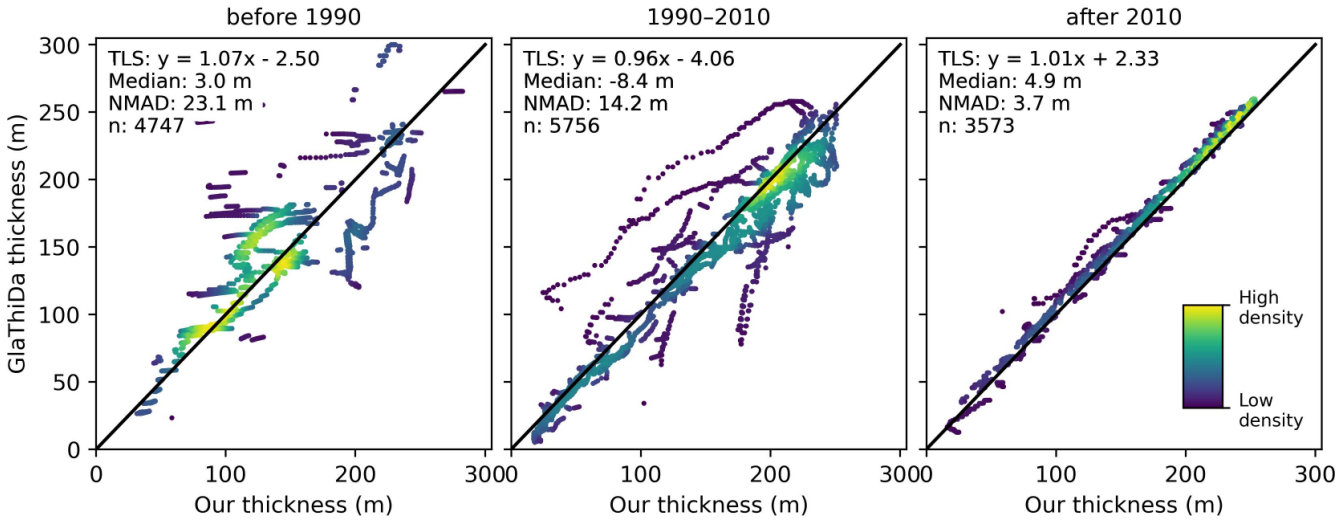

Figure 6. Glacier thickness measurements compared to previously published data in the Glacier Thickness Database (GlaThiDa) at points where previous data overlap, corrected for date disparity. The measurements are grouped by age, and statistics (median±NMAD) for each group are presented. The black line corresponds to a 1:1 ratio. "TLS" is the total least squares fit. Point color indicates point density (by a Gaussian kernel density estimate). The x-axis refers to the consensus estimate of our study.

differences clustering below the 1:1 line for all models. In addition, we observe a tendency to overestimate thin ice; we measure little to no ice in many areas where models predict ice thicknesses of >100 m. Our temporal thickness correction reduces the bias of all models by 20.5% on average, with an average NMAD improvement of 4.6% (cf. Fig. S2).

There is a variable dependence of inversion model performance on glacier thermal regime (Fig. 8). The median difference between cold and temperate beds (defined by whether it is overlain by temperate ice) is between -24.4 m and 13.3 m, depending on the model, which is well-within their overall uncertainty ranges. However, differences at individual glaciers can be larger than 100 m, and these differences may be both in positive and negative directions (Fig. 8, Fig. S4). While temperate ice presence is generally linked to elevation (accumulation areas typically contain more temperate ice than the lower ablation area), we observe no clear elevation dependence for cold vs. temperate bed performances (Fig. S5). This suggests that thermal regime — not elevation — explains the difference.

4 DISCUSSION

4.1 Bed and CTS interpretation uncertainty

Our crowd-sourced interpretation reveals a very high median consistency in terms of glacier bed picking (0.7±0.4 m). This is more than three times lower than the median calculated instrument uncertainty

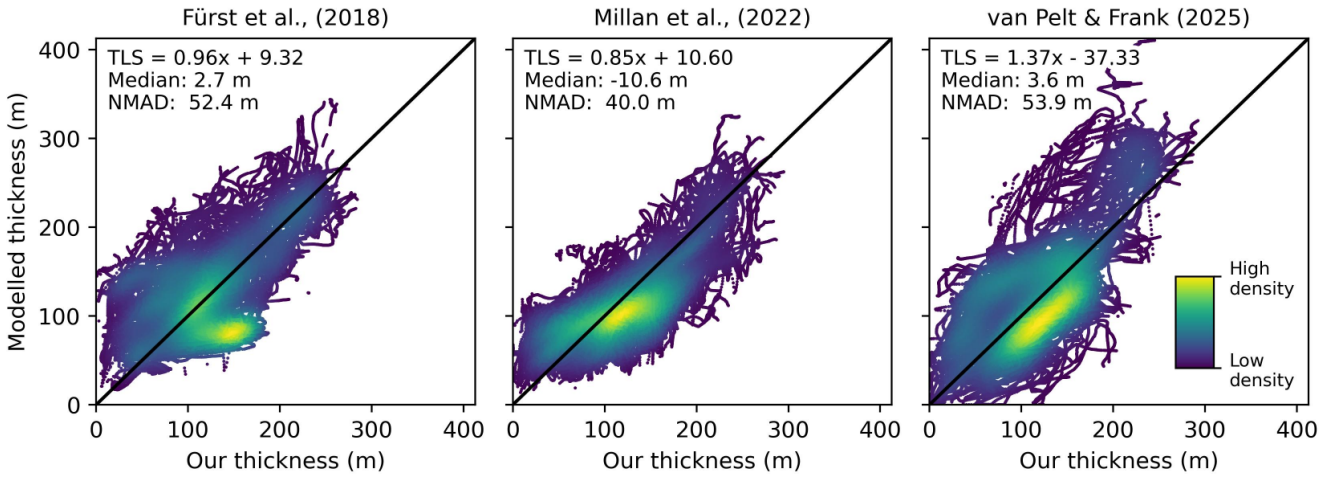

Figure 7. Glacier thickness measurements compared to thickness inversion models, corrected for date disparity. The black line corresponds to a 1:1 ratio. Positive median offsets represent a model overestimation. "TLS" is the total least squares fit. Point colour indicates point density (by a Gaussian kernel density estimate). The x-axis refers to the consensus estimate of our study.

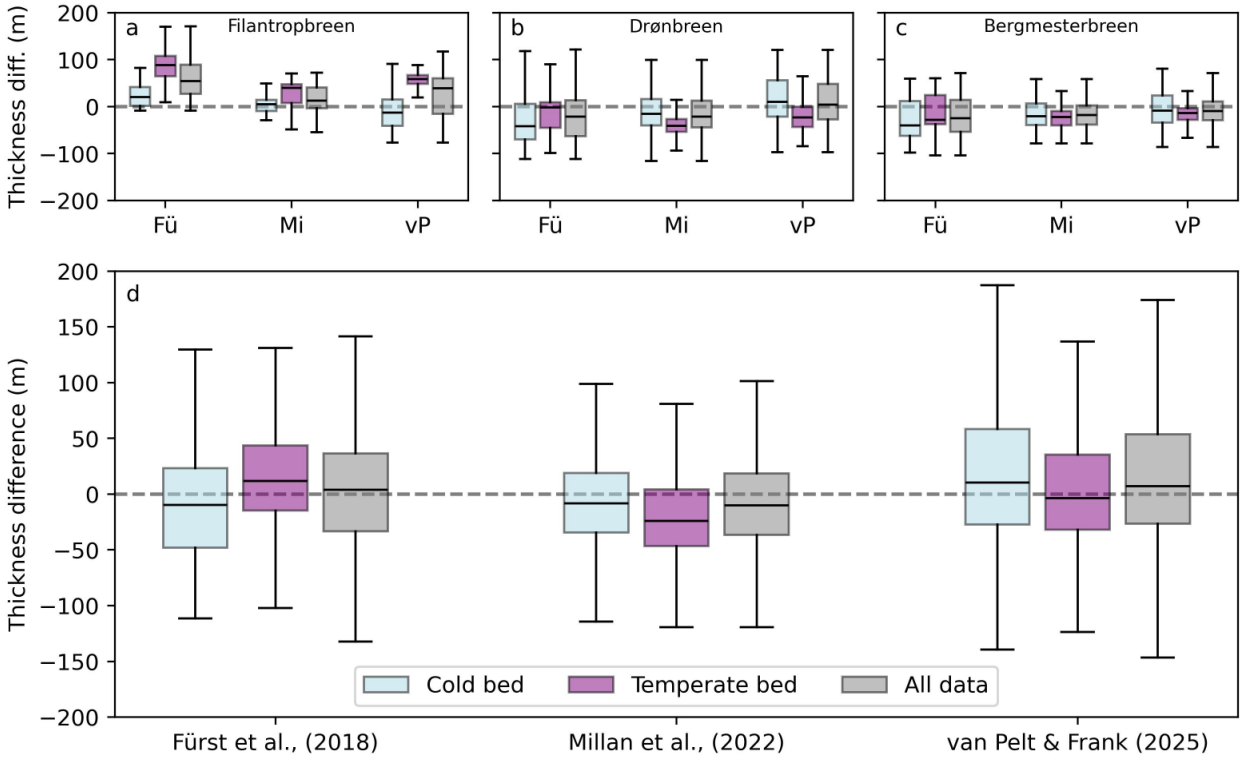

Figure 8. Thickness inversion model performance for temperate bed data, cold bed data, and all data. **a, b, c:** Example glaciers with variable performances based on inversion model and thermal regime. **d:** Differences for all glaciers in the study. All individual glacier performances can be seen in Figure S4. Positive differences represent a model overestimation.

(2.5±1.2 m) and about as large as the vertical effect of the positioning uncertainty (0.6±0.6 m). However, substantial deviations from the medians are evident. Multiple potentially off-nadir bed reflectors are a common challenge; for example, Figure 3j shows a radargram with two possible bed interpretations about 20 m apart in apparent thickness. Such ambiguity can occur because radio waves may reflect off side slopes, valley walls, englacial channels, steep bed sections, changes in bed slope, or surface debris and rocks (Plewes and Hubbard, 2001). In addition, there are a few cases where contributors disagreed on whether a reflection is the glacier bed or the CTS. Getting either of these wrong would increase the subjective uncertainty from 0.7 m to several tens of meters, making its magnitude substantially more important. About 1‰ of the data feature a subjective uncertainty of 20 m or higher, indicating that some areas needed a consensus estimate to reveal their ambiguity. Our study shows that ice thickness could be interpreted from most radargrams by a single qualified person and still be representative, assuming, however, that all uncertain areas are marked and treated differently. Even better, the parts with easily interpretable bed reflections — which make up most of the work — could be automated using statistical or machine learning methods, leaving human input for cases where interpretation is uncertain. Both future automated and manual approaches should be carried out with subjective uncertainty in mind, clearly defining where peer intervention may be required.

We observe disagreement among contributors regarding how much internal scattering indicates the upper boundary of temperate ice (CTS). This is expected, as contributors were requested to delineate a discrete boundary, despite it in reality being a gradual transition (Moorman and Michel, 2000; Pettersson and others, 2003). Areas like these have a high spread between the optimistic view on temperate ice fractions (the upper bound in the dataset) and the pessimistic view (the lower bound) (Fig. 3a-c). This is also reflected in the crossover analysis of the glacier bed and the CTS (Fig. 4), where the latter has a roughly six times higher spread. The problem arises mainly from the lack of a formal threshold of how much scattering should be considered as temperate ice, since we cannot extract the equivalent water content without inverse modelling (e.g. Ogier and others, 2023) or by other geophysical methods. Also, several features within the ice can cause scattering, and it can be challenging to distinguish whether it originates from temperate ice, sub- and englacial channels, or (water-filled) crevasses. Thus, our median CTS is a consensus estimate and not an exact threshold where the entrained liquid water content surpasses a certain percentage. Future work could be to apply statistical measures such as signal frequency response, internal reflective power, wavelet strength, or pattern matching (e.g. Schannwell and others, 2014; Delf and

others, 2022; Forte and others, 2025; Kachniarz and others, 2025), to formalise the definition of scattering indicative of temperate ice.

4.2 Processing and methodology limitations

The uncertainty patterns described above should be interpreted in light of several methodological choices. Our custom radar processing workflow enabled uniform processing of 138 radargrams, combined with 1498 individual crowd-sourced interpretations, but this batch processing came with some drawbacks. First, the bandpass filter and gain functions were applied identically to all radargrams, yet the bed visibility occasionally varied across different areas (cf. Fig. 3a and j). This may be due to inconsistencies in transmitted and received signals, variable bed scatter characteristics, or temperate ice — factors that may have been subverted through customised processing of individual profiles. Second, the use of a global time-zero correction based on the average trace, instead of a per-trace correction, introduced some drawbacks. In some radargrams, there is a clear jitter up and down due to a shifting zero-time, likely caused by fibre optic cable strain when driving over uneven terrain. However, this jitter is roughly equal in both positive and negative directions, which reduces radargram visibility but does not bias the interpretations. Third, we use only one radio-wave velocity throughout the dataset, despite it varying with the water content of the ice (Jania and others, 2005). According to the consensus estimate, 16% of our data are temperate, and these areas may therefore have a different, unknown velocity. Since the exact liquid water content of the temperate ice is not known, treating temperate ice differently would still be uncertain. Thus, we choose to only consider the issue by accounting for it in the uncertainty assessment (Eq. 1). Finally, although the uncertainty estimation approach of Lapazaran and others (2016) that we adopt is thorough, it is not fully comprehensive; for example, it does not account for the increasing spatial footprint of observations with increasing thickness. Future studies may therefore benefit from developing an even more comprehensive uncertainty assessment.

We speculate that the design of the crowd-sourcing website influences how interpretations are made, particularly through what information is provided to contributors. Our interface provided metadata on acquisition parameters, a satellite map showing the survey track, and the radargram without topographic correction. Interpretations were treated as lines, preventing tracking of individual point scatterers like water pockets. Many features would likely be interpreted differently depending on the contextual data and the labelling environment design. For example, supraglacial meltwater channels could be better distinguished

from temperate ice using satellite images; double bed reflectors could be explained by a V-shaped valley using DEMs, topographic maps, or an easier comparison environment between cross- and centreline-profiles; ice-cored moraines that may yield multiple internal reflections could be identified with glacier outlines and satellite images; and scatterers near the glacier terminus could potentially be recognised as entrained sediment with high-resolution imagery. There was also no possibility for the contributor to see individual trace plots or access quantitative amplitude or phase information. In addition, we have at least one example at Drønbreen of scatter appearing whilst passing a group of snowmobiles, which could subsequently be misinterpreted as crevassing or temperate ice. Such particular information was not available to the website users, supporting that familiarity with the data and study site may play a significant role. Altogether, radar interpretation is clearly more than signal waveform classification; it requires evaluation within its geographical and glaciological context. We therefore assume that our consensus estimate relies solely on the information provided on the website. Further site-specific analysis of our openly available data may be advantageous in future studies.

4.3 Comparisons with previous observations and inversion products

Our comparisons with previous observations and inversion products place our consensus estimates in a wider context and validates the agreement with previous data. To compare other sources fairly, we introduce a new and simple approach to temporally correct archival glacier thickness data by applying representative elevation change-based offsets; in our case, from 2000–2019 by Hugonnet and others (2021) and 1936–2010 by Geyman and others (2022). This correction reduced the pre-1990 and 1990–2010 spreads by almost half, and overall aligns the data closer to a 1:1 relationship between our data and archival data (cf. Figs. 6 and S1). However, the correction still does not lead to perfect fits. The comparison of data after 2010 has a median bias of 4.9 m (our data appearing thinner), which is close to the uncertainty range of the data, but could be affected by the 2019–2025 extrapolation of the elevation correction. Uncertainties remain especially in the predominantly airborne data from the 1980s, which may be a result of multiple effects: 1) our temporal thickness correction rates are not representative for archived 1980s data, 2) positioning-related uncertainties may exist in the 1980s flight lines (relying on satellite geoceivers and ground transponders, prior to modern GNSS), or 3) issues in digitising the archival data (using the wrong radio-wave velocity or miscalculating the time window). Without further analysis of the 1980s radargrams and positioning method, it is difficult to speculate further on the cause of the difference and we leave it for future studies. Nevertheless, correcting

thickness data with elevation change rates, which in our modern case are also globally available (Hugonnet and others, 2021), has proven to be a powerful tool for increasing the usefulness of archival thickness data.

The three glacier thickness inversion models that we tested generally perform within their own reported uncertainties at our measurement points. However, we observe glacier-specific differences beyond the reported uncertainties (Fig. S4), and an uneven distribution of differences to our data (Fig. 7), highlighting the need for further model development. First, a significant challenge is that the input datasets are often collected at different times, leading to inconsistencies (Millan and others, 2022; van Pelt and Frank, 2025). We recommend temporal correction of thickness measurements for calibration and validation, and reducing the temporal mismatch between glacier outlines, DEMs, and velocity fields to minimise errors. Second, representation of glacier surging remains limited in inversion models. Especially in Svalbard, where glacier surging is common, an optimal inversion approach would account for this explicitly. For example, using surges for thickness inversion (Morin and others, 2023) or at least treating them differently (van Pelt and Frank, 2025) are clearly advantageous directions. Finally, we observe a bias difference ranging from -24.4 m to 13.3 m between cold and temperate beds for glacier thickness inversion performance. This is most likely due to the regional flow and sliding parameter calibrations, which fail to capture the variable thermal regime of individual glaciers. Accounting for this would be challenging without even more available data on glacier thermal regime, but it may be necessary for optimal inversion performance. Machine learning approaches could potentially learn patterns related to thermal regime to exclude the anisotropy problem entirely (e.g. Maffezzoli and others, 2025; Steidl and others, 2025).

4.4 Thermal regime and glacier dynamics

The consensus CTS estimates reveal notable differences in thermal regime geometry between glaciers, including steep transitions from cold termini to temperate accumulation areas in selected centreline profiles (14–34°). Several of the steepest transitions occur on glaciers with recent, historical or suspected upcoming surge-related behaviour, suggesting that CTS geometry may be a useful variable for understanding transient glacier dynamics. To emphasise the magnitude of this steepness, we measured the transition angle to 1–2° from the published CTS figures of Bakaninbreen from Murray and others (1998), who provided the empirical basis for thermally regulated surging (Fowler and others, 2001). This contrast suggests that thermal regulation of surge-like behaviour may involve stronger thermal gradients than previously assumed. The steep transitions observed here could represent different stages of dynamic and climatic adjustment, or

glacier-specific geometric controls, but the temporal snapshot that our data represents is likely insufficient to fully understand the implications of our findings. Repeated GPR surveys, surface elevation change studies, and thermomechanical modelling are future potential pathways which may constrain the plausible explanations for this interesting phenomenon.

4.5 Data sharing and future automation

Within this study, we openly share our raw, processed, and interpreted GPR data from 25 glaciers in Svalbard. This was enabled by the archiving of raw data, common data processing, and the impressively consistent interpretation efforts by our 41 contributors over 30 institutions and 12 countries. In general, a wider diversity of processing and interpretation approaches would be enabled by more data sharing of glacier thickness, CTS observations, and other variables. The ice-sheet radioglaciology community already provides both openly available data and labels (picked horizons) to test new approaches for internal layer tracing (Moqadam and Eisen, 2025; Moqadam and others, 2025; Dreier and others, 2025; Young and others, 2025). Progress on automation has also been made in Svalbard (Schannwell and others, 2014; Kachniarz and others, 2025), but this has not been employed at scale yet. An optimal starting point would be a large repository of both radargrams and labels for models to be trained and tested on; especially for machine learning as training often requires high data volumes. Some examples of either open radargrams or bed/CTS picks exist for Svalbard glaciers (Grabiec, 2017; Delf and others, 2022; Grabiec, 2025), but unfortunately not both for the same data. In addition, modern thickness inversion models require more in situ measurements to improve performance (Fürst and others, 2018), and local studies may need data in ways that are not yet conceived. Adding more open data is evidently a step forward in terms of making many types of research accessible and for accelerating their progress.

5 CONCLUSION

We present new GPR data from 25 glaciers in Svalbard covering 699 km, and obtain glacier thickness and thermal regime profiles by crowd-sourcing interpretations from the glaciological community. Our new thickness profiles agree well with previously published data, especially after temporally correcting the older data using DEM-based elevation change information. The calculated total uncertainty of glacier thickness (median±NMAD between points) is 3.0±1.2 m, which is mainly dictated by instrument error rather than the median interpretation consensus variability of 0.7±0.4 m. This indicates that manual

bed interpretation can be highly repeatable for clear ground-based GPR profiles, but only if ambiguous sections are identified and treated explicitly. Exceptions occur where multiple bed reflectors, off-nadir reflections, or substantial temperate ice complicate interpretation. Thermal regime estimates were mapped less consistently than the glacier bed, with a subjective CTS uncertainty of 6.2±4.3 m, and subjective differences in what is considered enough scattering to indicate temperate ice. This highlights the need for more indicators beyond only visible scattering to reliably delineate the CTS in radargrams.

Our consensus estimates of thermal regime indicate a large variability in internal configurations. We measure many steep (14–34°) cold-to-temperate transition zones at glaciers with surge-related behaviour, and studying this relationship is a potential avenue for future research. We also test recent glacier thickness inversion models which show indications of a thermal regime-dependence on their performance, and a large per-glacier variability, emphasising its importance to consider for future research. Transient modelling of thermal regime and evolution is clearly essential to fully understand our observed patterns, and we advocate this direction with the data that we share.

Our results suggest that a hybrid interpretation strategy for glacier radar interpretation may be optimal for future work. Clear glacier bed reflections can often be interpreted manually by a single qualified operator with low subjective uncertainty, or potentially be automated with the same effect. In contrast, ambiguous bed sections and CTS picks require explicit uncertainty reporting and, ideally, multiple interpretations or automated outputs that return a range of possibilities rather than one discrete line. Automation in glacier bed and CTS detection would speed up processing and improve consistency, but it should be implemented in a way that transparently acknowledges parts that may be ambiguous. Finally, while our results suggest that subjective uncertainties are generally low for bed picks in these data, the reported magnitudes are only directly applicable to similar ground-based acquisitions and should not be assumed for all radar survey types.

SUPPLEMENTARY MATERIAL

The supplementary material for this article can be found at (link).

DATA AVAILABILITY

An archived version of the radar interpretation website can be found at `https://erikmannerfelt.github.io/svalbard_radar_web`. The code for the analysis is available at `https://github.com/erikmannerfelt/`

`svalbard_radar`. The radar processing software *ridal* is available at `https://github.com/erikmannerfelt/ridal`. A data publication of raw, processed, and interpreted data, including co-registered DEMs, is available at `https://doi.org/10.5281/zenodo.17882299`.

AUTHOR CONTRIBUTIONS

ESM initiated and designed the study, compiled and curated the datasets, built the website, performed the data analyses, and generated the figures. ESM interpreted the results and wrote the manuscript with significant input from SI, JA, KP, and UE. All authors commented and contributed to the clarity of the manuscript. Data were mainly collected by ESM and UE, along with data from SS, SI, JA, MKG, and AH, and substantial field assistance by GK, JK, and GM. SI coordinated the contributor communication and website support. ESM and JB designed the consensus algorithm. ESM, SI, GK, KP, JA, JK, SS, UE, MKG, AH, and GM contributed to the radar interpretations.

ACKNOWLEDGEMENTS

ESM and UE were supported by Research Council of Norway Arctic Field Grants (NFR ids: 350271 and 350454, respectively). Field activities on Nordaustlandet were carried out as part of the Austfonna mass balance program by the Norwegian Polar Institute and the University of Oslo, with additional funding from the European Space Agency project, St3TART. JB was funded by ERC-2022-ADG grant 101096057 (GLACMASS). GK and AH were supported by Research Council of Norway grants CLIMAGAS (NFR id: 294764), GLACIGAS (NFR id: 343293) and HYDRO-SURGE (NFR id: 329174). We thank the University Centre in Svalbard (UNIS) and the Norwegian Polar Institute for logistic support. We thank everyone partaking in the UNIS Glaciology (AG-325/825) course data acquisition, and Joe Buckby, Audun Tholfsen, Heïdi Sevestre, John Hulth, Alexander Maschler, and Wilson Cheung for assistance in the field. Thank you Andreas Kääb for overall guidance. Thank you Clemens Schannwell and one anonymous reviewer for feedback that improved the state of the manuscript.

We are grateful to all the contributors who participated in interpreting the radargrams: Ward van Pelt, Per Holmlund, Emanuele Forte, Thomas Loriaux, Celine Madsen, Moritz Koch, Antoine Rabatel, Mélissa Francey, Emma Skelton, Clément Cherblanc, Pernille Line Ottosen, Michele Pipan, Caroline Dalhaug, Gwenn Flowers, Zhuo Wang, Jason Drebber, Christophe Ogier, Jan Magne Cederstrøm, Adam Garbo, Iestyn Barr, David Farías-Barahona, Armin Dachauer, Mikaila Mannello, Jakob Gradl, Ilaria Santin, Renée

Clavette, Marjolein Gevers, Keeya Beausoleil, Paula Johns, and Marlene Schramm.

REFERENCES

Bælum K and Benn DI (2011) Thermal structure and drainage system of a small valley glacier (Tellbreen, Svalbard), investigated by ground penetrating radar. *The Cryosphere*, **5**(1), 139–149 (doi: 10.5194/tc-5-139-2011)

Björnsson H, Gjessing Y, Hamran SE, Hagen JO, Liestøl O, Pálsson F and 1 other (1996) The thermal regime of sub-polar glaciers mapped by multi-frequency radio-echo sounding. *Journal of Glaciology*, **42**(140), 23–32 (doi: 10.3189/S0022143000030495)

Borisik A, Novikov A, Lavrentiev I and Glazovsky A (2022) Changes in the internal structure of polythermal glaciers over the last decade: the case study of Fridtjofbreen and Erdmanbreen from 2010 to 2021, Svalbard (doi: 10.5194/egusphere-egu22-1852)

Bradford JH, Nichols J, Mikesell TD and Harper JT (2009) Continuous profiles of electromagnetic wave velocity and water content in glaciers: an example from Bench Glacier, Alaska, USA. *Annals of Glaciology*, **50**(51), 1–9 (doi: 10.3189/172756409789097540)

Copland L and Sharp M (2001) Mapping thermal and hydrological conditions beneath a polythermal glacier with radio-echo sounding. *Journal of Glaciology*, **47**(157), 232–242 (doi: 10.3189/172756501781832377)

Cuffey K and Paterson WSB (2010) *The Physics of Glaciers*. Butterworth-Heinemann/Elsevier, Burlington, MA, 4th ed edition, ISBN 978-0-12-369461-4, oCLC: ocn488732494

Delf R, Bingham RG, Curtis A, Singh S, Giannopoulos A, Schwarz B and 1 other (2022) Reanalysis of Polythermal Glacier Thermal Structure Using Radar Diffraction Focusing. *Journal of Geophysical Research: Earth Surface*, **127**(2), e2021JF006382 (doi: 10.1029/2021JF006382)

Dowdeswell J, Drewry D, Cooper A, Gorman M, Liestøl O and Orheim O (1986) Digital Mapping of the Nordaustlandet Ice Caps from Airborne Geophysical Investigations. *Annals of Glaciology*, **8**, 51–58 (doi: 10.3189/S0260305500001130)

Dowdeswell JA, Drewry DJ, Liestøl O and Orheim O (1984) *Airborne radio echo sounding of sub-polar glaciers in Spitsbergen*, volume 182. Norsk Polarinstitutt Skrifter, Oslo

Dreier M, Koch M, Gourmelon N, Blindow N, Steinhage D, Wu F and 4 others (2025) IceAnatomy: a benchmark dataset and methodology for automatic ice boundary extraction from radio-echo sounding data. *The Cryosphere*, **19**(11), 5337–5359 (doi: 10.5194/tc-19-5337-2025)

Farinotti D, Huss M, Fürst JJ, Landmann J, Machguth H, Maussion F and 1 other (2019) A consensus estimate for the ice thickness distribution of all glaciers on Earth. *Nature Geoscience*, **12**(3), 168–173 (doi: 10.1038/s41561-019-0300-3)

Forte E, Gutgesell P, Securo A, Marcer M, Citterio M, Machguth H and 1 other (2025) Comparing GPR with ice thickness and thermal models: Insights from two polythermal glaciers in West Greenland. *Journal of Glaciology*, **71**, e97 (doi: 10.1017/jog.2025.10067)

Fowler AC, Murray T and Ng FSL (2001) Thermally controlled glacier surging. *Journal of Glaciology*, **47**(159), 527–538 (doi: 10.3189/172756501781831792)

Fürst JJ, Navarro F, Gillet-Chaulet F, Huss M, Moholdt G, Fettweis X and 20 others (2018) The Ice-Free Topography of Svalbard. *Geophysical Research Letters*, **45**(21), 11,760–11,769 (doi: 10.1029/2018GL079734)

Gades AM, Raymond CF, Conway H and Jagobel RW (2000) Bed properties of Siple Dome and adjacent ice streams, West Antarctica, inferred from radio-echo sounding measurements. *Journal of Glaciology*, **46**(152), 88–94 (doi: 10.3189/172756500781833467)

Geyman EC, van Pelt WJJ, Maloof AC, Faste Aas H and Kohler J (2022) Historical glacier change on Svalbard predicts doubling of mass loss by 2100. *Nature*, **601**, 374–395 (doi: 10.1038/s41586-021-04314-4)

Grabiec M (2017) *Stan i współczesne zmiany systemów lodowcowych południowego Spitsbergenu w świetle badań metodami radarowymi*. Number nr 3536 in Prace Naukowe Uniwersytetu Śląskiego w Katowicach, Wydawnictwo Uniwersytetu Śląskiego, Katowice, ISBN 978-83-226-3014-3 978-83-226-3015-0

Grabiec M (2025) GPR input data (2007-2021) and processing code for recognitition of Hansbreen internal structure

Guillet G, Benn D, King O, Shean D, Schytt Mannerfelt E and Hugonnet R (2025) Global detection of glacier surges from surface velocities, elevation change, and SAR backscatter data between 2000 and 2024: a test of surge mechanism theories. *Journal of Glaciology*, **71**(e88) (doi: 10.1017/jog.2025.10065)

Gusmeroli A, Jansson P, Pettersson R and Murray T (2012) Twenty years of cold surface layer thinning at Storglaciären, sub-Arctic Sweden, 1989-2009. *Journal of Glaciology*, **58**(207), 3–10 (doi: 10.3189/2012JoG11J018)

Gärtner-Roer I, Naegeli K, Huss M, Knecht T, Machguth H and Zemp M (2014) A database of worldwide glacier thickness observations. *Global and Planetary Change*, **122**, 330–344 (doi: 10.1016/j.gloplacha.2014.09.003)

Hagen JO, Liestøl O, Roland E and Jørgensen T (eds.) (1993) *Glacier atlas of Svalbard and Jan Mayen*. Number 129 in Meddelelser / Norsk Polarinstitutt, Nork Polarinstitutt, Oslo, ISBN 978-82-7666-066-1, oCLC: 612170272

Hamran S and Aarholt E (1993) Glacier study using wavenumber domain synthetic aperture radar. *Radio Science*, **28**(4), 559–570 (doi: 10.1029/92RS03022)

Harcourt WD, Pearce DM, Gajek W, Lovell H, Luckman A, Benn D and 3 others (2025) Surging glaciers in Svalbard: Current knowledge and perspectives for monitoring (SvalSurge). Technical report, Svalbard Integrated Arctic Earth Observing System (doi: 10.5281/ZENODO.14425522)

Hugonnet R, McNabb R, Berthier E, Menounos B, Nuth C, Girod L and 5 others (2021) Accelerated global glacier mass loss in the early twenty-first century. *Nature*, **592**(7856), 726–731 (doi: 10.1038/s41586-021-03436-z)

Irvine-Fynn TDL, Moorman BJ, Williams JLM and Walter FSA (2006) Seasonal changes in ground-penetrating radar signature observed at a polythermal glacier, Bylot Island, Canada. *Earth Surface Processes and Landforms*, **31**(7), 892–909 (doi: 10.1002/esp.1299)

Jacquemart M, Welty E, Gastaldello M and Carcanade G (2025) glenglat: a database of global englacial temperatures. *Earth System Science Data*, **17**(4), 1627–1666 (doi: 10.5194/essd-17-1627-2025)

Jania J, Mochnacki D and Gadek B (1996) The thermal structure of Hansbreen, a tidewater glacier in southern Spitsbergen, Svalbard. *Polar Research*, **15**(1), 53–66 (doi: 10.1111/j.1751-8369.1996.tb00458.x)

Jania J, Macheret Y, Navarro F, Glazovsky A, Vasilenko E, Lapazaran J and 4 others (2005) Temporal changes in the radiophysical properties of a polythermal glacier in Spitsbergen. *Annals of Glaciology*, **42**, 125–134 (doi: 10.3189/172756405781812754)

Kääb A, Bazilova V, Leclercq PW, Mannerfelt ES and Strozzi T (2023) Global clustering of recent glacier surges from radar backscatter data, 2017–2022. *Journal of Glaciology*, 1–9 (doi: 10.1017/jog.2023.35)

Kachniarz K, Grabiec M, Wróbel K and Ignatiuk D (2025) Glacier internal structure revealed by automatic image processing-powered classification of radar images. *Applied Geomatics*, **17**(4), 677–692 (doi: 10.1007/s12518-025-00635-5)

Karušs J, Lamsters K, Sobota I, Ješkins J, Džeriņš P and Hodson A (2022) Drainage system and thermal structure of a High Arctic polythermal glacier: Waldemarbreen, western Svalbard. *Journal of Glaciology*, **68**(269), 591–604 (doi: 10.1017/jog.2021.125)

Lapazaran J, Otero J, Martín-Español A and Navarro F (2016) On the errors involved in ice-thickness estimates I: ground-penetrating radar measurement errors. *Journal of Glaciology*, **62**(236), 1008–1020 (doi: 10.1017/jog.2016.93)

Leys C, Ley C, Klein O, Bernard P and Licata L (2013) Detecting outliers: Do not use standard deviation around the mean, use absolute deviation around the median. *Journal of Experimental Social Psychology*, **49**(4), 764–766 (doi: 10.1016/j.jesp.2013.03.013)

Macheret Y, Glazovsky A and Lavrentiev I (2019) Distribution of cold and temperate ice and water in glaciers at Nordenskiöld Land, Svalbard, according to data on ground-based radio-echo sounding. *Bulletin of Geography. Physical Geography Series*, **17**(1), 77–90 (doi: 10.2478/bgeo-2019-0016)

Macheret YY and Zhuravlev AB (1982) Radio Echo-Sounding of Svalbard Glaciers. *Journal of Glaciology*, **28**(99), 295–314 (doi: 10.3189/S0022143000011643)

Maffezzoli N, Rignot E, Barbante C, Petersen T and Vascon S (2025) A gradient-boosted tree framework to model the ice thickness of the world's glaciers (IceBoost v1.1). *Geoscientific Model Development*, **18**(9), 2545–2568 (doi: 10.5194/gmd-18-2545-2025)

Mannerfelt ES, Dehecq A, Hugonnet R, Hodel E, Huss M, Bauder A and 1 other (2022) Halving of Swiss glacier volume since 1931 observed from terrestrial image photogrammetry. *The Cryosphere*, **16**(8), 3249–3268 (doi: 10.5194/tc-16-3249-2022)

Mannerfelt ES, Hodson AJ, Håkansson L and Lovell H (2024) Dynamic LIA advances hastened the demise of small valley glaciers in central Svalbard. *Arctic Science*, as–2024–0024 (doi: 10.1139/as-2024-0024)

Mannerfelt ES, Schellenberger T and Kääb AM (2025) Tracking glacier surge evolution using interferometric SAR coherence – examples from Svalbard. *Journal of Glaciology*, **71**, 1–17 (doi: 10.1017/jog.2025.27)

Meier MF and Post A (1969) What are glacier surges? *Canadian Journal of Earth Sciences*, **6**(4), 807–817 (doi: 10.1139/e69-081)

Millan R, Mouginot J, Rabatel A and Morlighem M (2022) Ice velocity and thickness of the world's glaciers. *Nature Geoscience*, **15**(2), 124–129 (doi: 10.1038/s41561-021-00885-z)

Moorman BJ and Michel FA (2000) Glacial hydrological system characterization using ground-penetrating radar. *Hydrological Processes*, **14**(15), 2645–2667

Moqadam H and Eisen O (2025) Review article: Feature tracing in radio-echo sounding products of terrestrial ice sheets and planetary bodies. *The Cryosphere*, **19**(6), 2159–2196 (doi: 10.5194/tc-19-2159-2025)

Moqadam H, Steinhage D, Wilhelm A and Eisen O (2025) Going Deeper With Deep Learning: Automatically Tracing Internal Reflection Horizons in Ice Sheets—Methodology and Benchmark Data Set. *Journal of Geophysical Research: Machine Learning and Computation*, **2**(2), e2024JH000493 (doi: 10.1029/2024JH000493)

Morin A, Flowers GE, Nolan A, Brinkerhoff D and Berthier E (2023) Exploiting high-slip flow regimes to improve inference of glacier bed topography. *Journal of Glaciology*, **69**(275), 658–664 (doi: 10.1017/jog.2022.121)

Murray T, Dowdeswell JA, Drewry DJ and Frearson I (1998) Geometric evolution and ice dynamics during a surge of Bakaninbreen, Svalbard. *Journal of Glaciology*, **44**(147), 263–272 (doi: 10.3189/S0022143000002604)

Navarro F, Möller R, Vasilenko E, Martín-Español A, Finkelnburg R and Möller M (2015) Ice thickness distribution and hydrothermal structure of Elfenbeinbreen and Sveigbreen, eastern Spitsbergen, Svalbard. *Journal of Glaciology*, **61**(229), 1015–1018 (doi: 10.3189/2015JoG15J141)

Norwegian Polar Institute (2014a) Kartdata Svalbard 1:100 000 (S100 Kartdata) / Map Data (doi: 10.21334/NPOLAR.2014.645336C7)

Norwegian Polar Institute (2014b) Terrengmodell Svalbard (S0 Terrengmodell) (doi: 10.21334/npolar.2014.dce53a47)

Nuth C and Kääb A (2011) Co-registration and bias corrections of satellite elevation data sets for quantifying glacier thickness change. *The Cryosphere*, **5**(1), 271–290 (doi: 10.5194/tc-5-271-2011)

Nuth C, Kohler J, König M, von Deschwanden A, Hagen JO, Kääb A and 2 others (2013) Decadal changes from a multi-temporal glacier inventory of Svalbard. *The Cryosphere*, **7**(5), 1603–1621 (doi: 10.5194/tc-7-1603-2013)

Ogier C, Van Manen DJ, Maurer H, Räss L, Hertrich M, Bauder A and 1 other (2023) Ground penetrating radar in temperate ice: englacial water inclusions as limiting factor for data interpretation. *Journal of Glaciology*, 1–12 (doi: 10.1017/jog.2023.68)

Paden J, Li J, Leuschen C, Rodriguez-Morales F and Hale R (2010) IceBridge MCoRDS L2 Ice Thickness, Version 1 (doi: 10.5067/GDQ0CUCVTE2Q)

Pettersson R, Jansson P and Holmlund P (2003) Cold surface layer thinning on Storglaciären, Sweden, observed by repeated ground penetrating radar surveys: COLD SURFACE LAYER THINNING ON STORGLACIÄREN. *Journal of Geophysical Research: Earth Surface*, **108**(F1), n/a–n/a (doi: 10.1029/2003JF000024)

Plewes LA and Hubbard B (2001) A review of the use of radio-echo sounding in glaciology. *Progress in Physical Geography: Earth and Environment*, **25**(2), 203–236 (doi: 10.1177/030913330102500203)

Porter C, Morin P, Howat I, Noh MJ, Bates B, Peterman K and 23 others (2018) ArcticDEM (doi: 10.7910/DVN/OHHUKH)

Schannwell C, Murray T, Kulessa B, Gusmeroli A, Saintenoy A and Jansson P (2014) An automatic approach to delineate the cold–temperate transition surface with ground-penetrating radar on polythermal glaciers. *Annals of Glaciology*, **55**(67), 89–96 (doi: 10.3189/2014AoG67A102)

Schlegel R, Kulessa B, Murray T and Eisen O (2022) Towards a common terminology in radioglaciology. *Annals of Glaciology*, **63**(87-89), 8–12 (doi: 10.1017/aog.2023.2)

Schuler T and Melvold K (2004) Melt water production at Gruvefonna and subglacial water intrusions into Svea Nord Gruva. Technical report, Institutt for geofag, avdeling for Naturgeografi, Universitetet i Oslo

Sevestre H and Benn DI (2015) Climatic and geometric controls on the global distribution of surge-type glaciers: implications for a unifying model of surging. *Journal of Glaciology*, **61**(228), 646–662 (doi: 10.3189/2015JoG14J136)

Sevestre H, Benn DI, Hulton NRJ and Baelum K (2015) Thermal structure of Svalbard glaciers and implications for thermal switch models of glacier surging. *Journal of Geophysical Research: Earth Surface*, **120**(10), 2220–2236 (doi: 10.1002/2015JF003517)

Steidl V, Bamber JL and Zhu XX (2025) Physics-aware machine learning for glacier ice thickness estimation: a case study for Svalbard. *The Cryosphere*, **19**(2), 645–661 (doi: 10.5194/tc-19-645-2025)

Sund M, Eiken T, Hagen JO and Kääb A (2009) Svalbard surge dynamics derived from geometric changes. *Annals of Glaciology*, **50**(52), 50–60 (doi: 10.3189/172756409789624265)

van Pelt W and Frank T (2025) New glacier thickness and bed topography maps for Svalbard. *The Cryosphere*, **19**(1), 1–17 (doi: 10.5194/tc-19-1-2025)

Vasilenko E, Navarro F, Dunse T, Eiken T, Hagen J and Moholdt G (2009) New low-frequency radio-echo soundings of Austfonna ice cap, Svalbard. In AP Ahlstrøm and M Sharp (eds.), *Extended Abstracts, Workshop and GLACIODYN (IPY) Meeting*, 64–67, Kananaskis, Canada

Welty E, Zemp M, Navarro F, Huss M, Fürst JJ, Gärtner-Roer I and 7 others (2020) Worldwide version-controlled database of glacier thickness observations. *Earth System Science Data*, **12**(4), 3039–3055 (doi: 10.5194/essd-12-3039-2020)

Wilson NJ, Flowers GE and Mingo L (2014) Mapping and interpretation of bed-reflection power from a surge-type polythermal glacier, Yukon, Canada. *Annals of Glaciology*, **55**(67), 1–8 (doi: 10.3189/2014AoG67A101)

xdem contributors (2021) xdem (doi: 10.5281/ZENODO.4809697)

Young DA, Paden JD, Yan S, Kerr ME, Singh S, Vega González A and 7 others (2025) Coupled Ice Sheet Structure and Bedrock Geology in the Deep Interior of East Antarctica: Results From Dome A and the South Pole Basin. *Geophysical Research Letters*, **52**(19), e2025GL115729 (doi: 10.1029/2025GL115729)

Ødegård RS, Hagen JO and Hamranw SE (1997) Comparison of radio-echo sounding (30–1000 MHz) and high-resolution borehole-temperature measurements at Finsterwalderbreen, southern Spitsbergen, Svalbard. *Annals of Glaciology*, **24**, 262–267 (doi: 10.3189/S0260305500012271)

SUPPLEMENTARY MATERIAL

Supplementary Text

On the use of migration

We do not use migration when processing the radargrams for a number of reasons. Bed slopes (rates of thickness change) are generally low (25th percentile: 0.89°, median: 2.38°, 75th: 4.02°), and temperate ice is easier to identify in unmigrated radargrams. In addition, driving speeds and directions in relation to bed topography were not consistent enough to enable a fully two-dimensional analysis (limiting the use of F-K or Kirchhoff implementations). Finally, we wanted the crowd-sourced interpretations to be as future-proof as possible. Since different migration approaches and implementations modify the data differently, we therefore opt to not make the interpretations implementation-specific.

Supplementary Figures

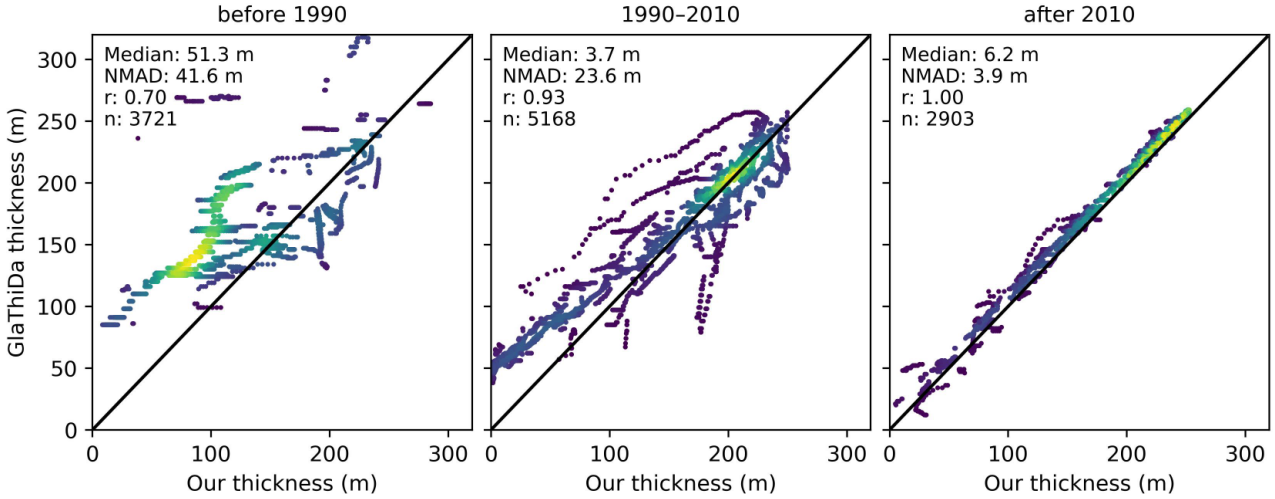

Figure S1. Uncorrected glacier thickness measurements compared to previously published data in the Glacier Thickness Database (GlaThiDa) at points where previous data overlap. This is identical to Figure 5 in the main text except no temporal thickness correction has been made here.

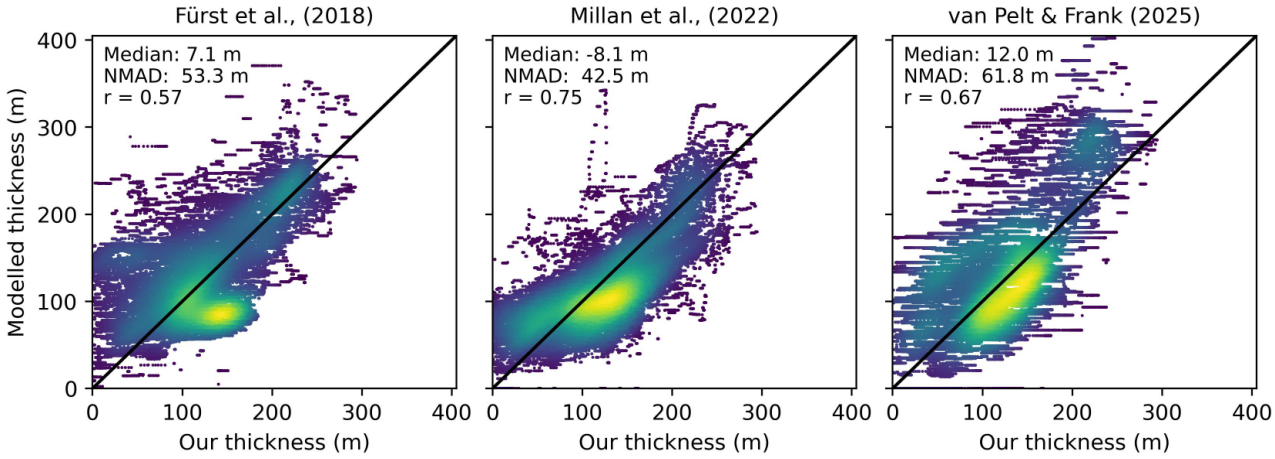

Figure S2. Uncorrected glacier thickness measurements compared to thickness models. This is identical to Figure 6 in the main text except no temporal thickness correction has been made.

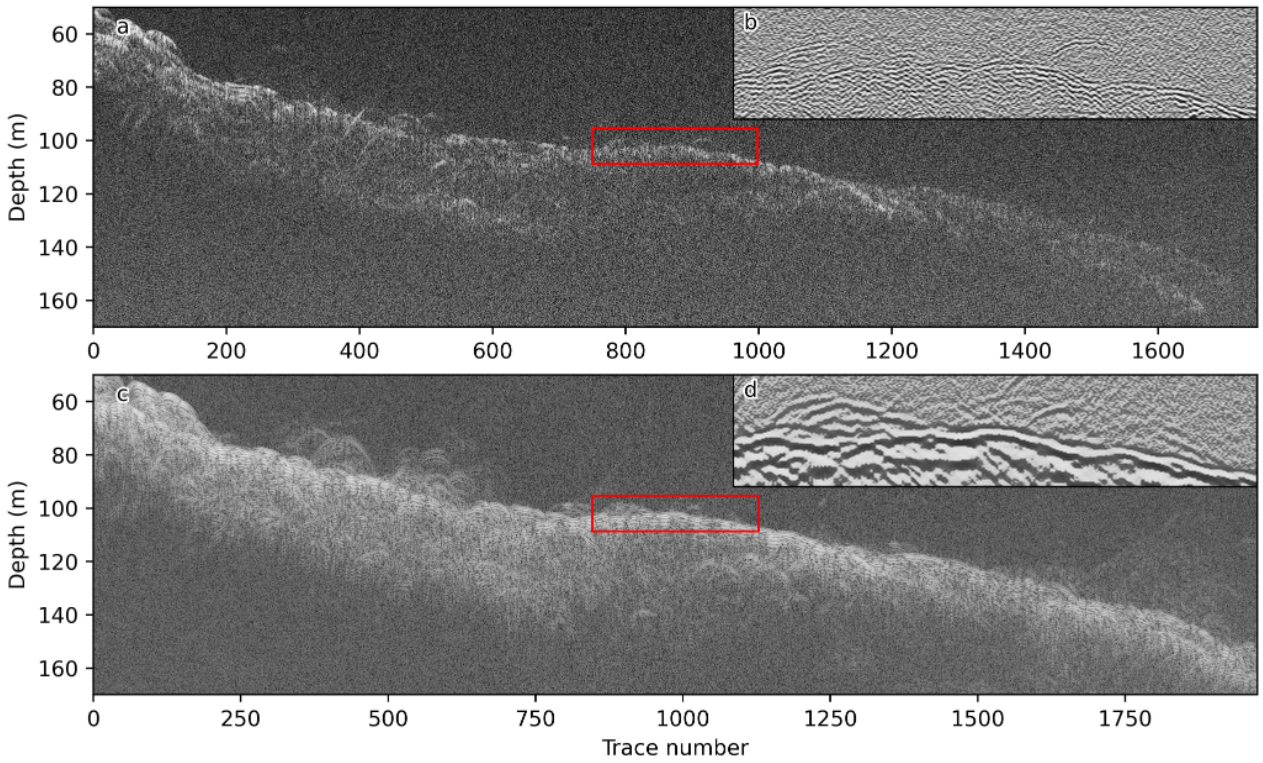

Figure S3. Visual comparison of bed reflections at different frequencies near the front of Ragna-Mariebreen. **a:** Radargram with a 100 MHz centre frequency (absolute values) and an inset in red referring to **b:** zoomed view of the same data (signed values). **c:** Radargram of the same line at 25 MHz and **d:** an equivalent zoomed view. The total profile length is 1590 m.

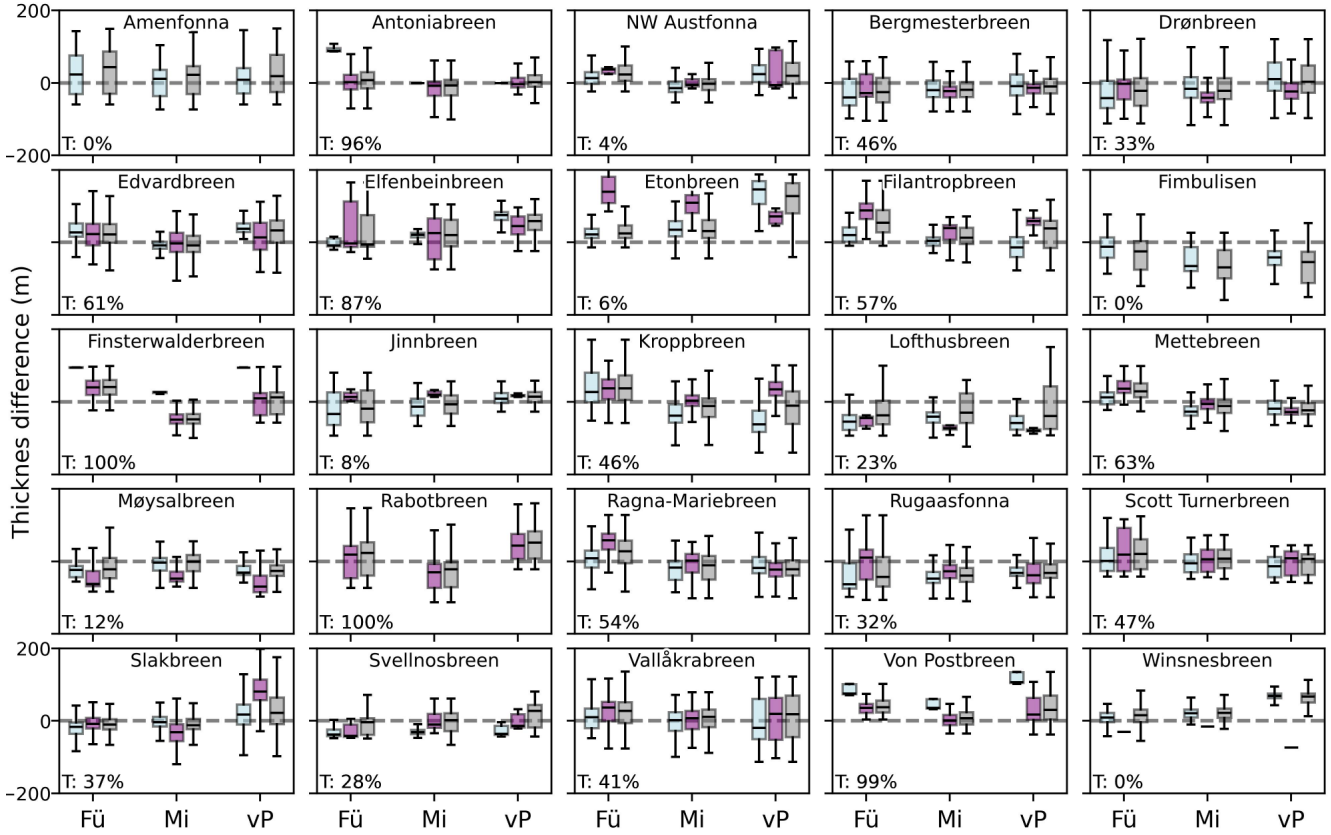

Figure S4. Thickness inversion model differences between temperate and cold beds for each glacier individually (extends Figure 7). The "T" in the lower right corner stands for the fraction of the bed that is classified as temperate (comparisons closer to 50% are more representative). The inversion models refer to Fü: Fürst and others (2018), Mi: Millan and others (2022), and vP: Van Pelt and Frank (2025).

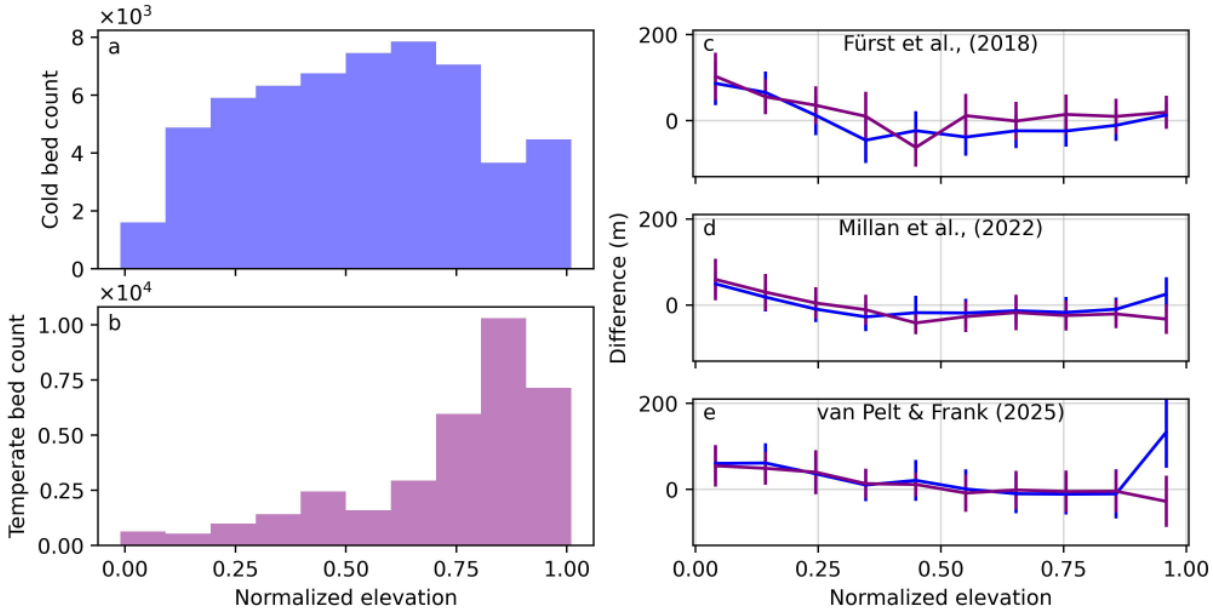

Figure S5. Differences between modelled and measured glacier thickness under cold and temperate conditions, plotted against normalized elevation. **a:** Distribution of cold bed points, **b:** distribution of temperate bed points, and **c,d,e:** thickness difference under these two conditions. There is a clear model overestimation at low elevations, and a visible but not order-of-magnitude difference between cold and temperate bed performance.

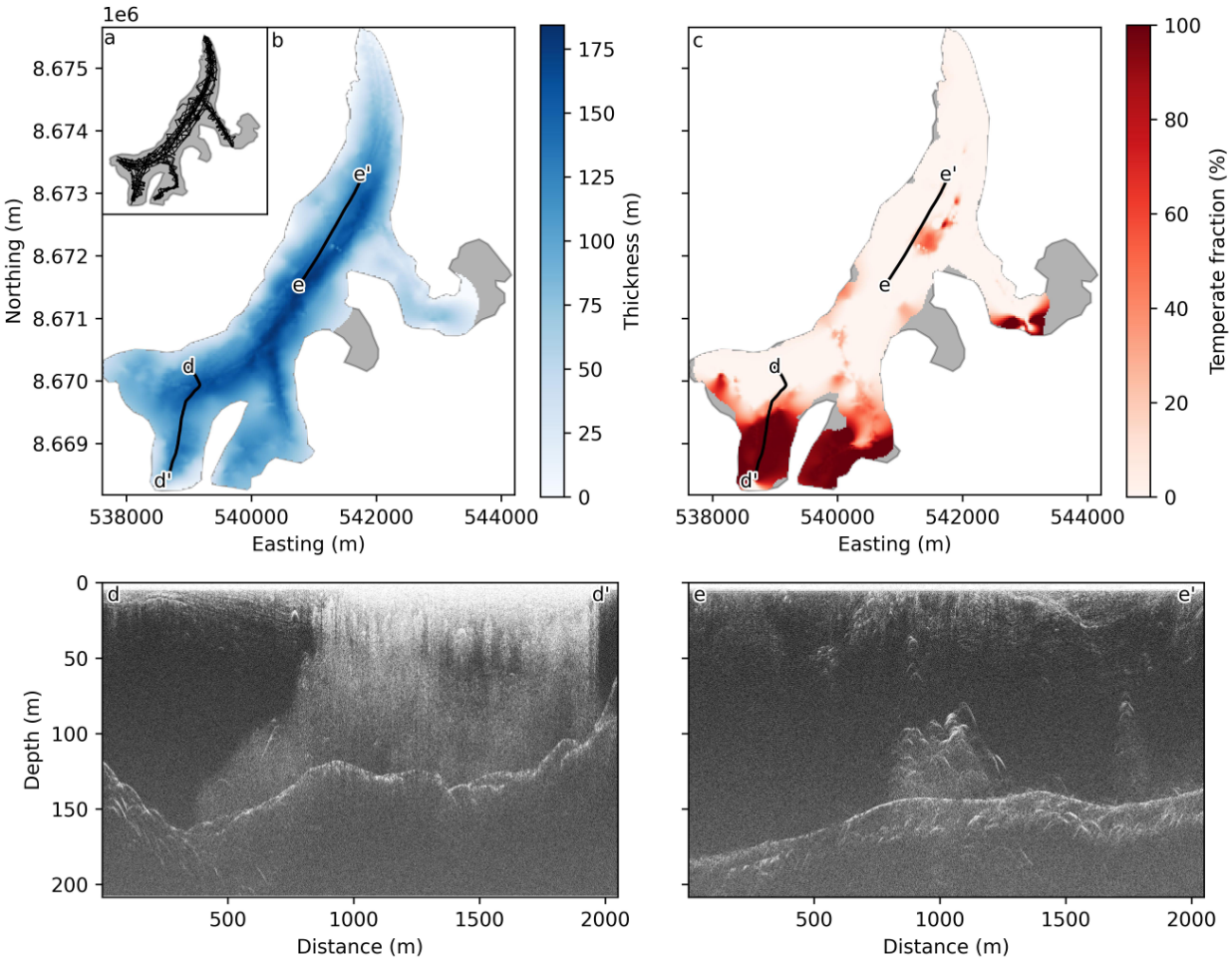

Figure S6. Examples of data for Drønbreen: **a**: all survey tracks, **b**: interpolated thickness (using RBF interpolation), and **c**: interpolated temperate ice fraction. Radargrams (lines in **b** and **c**) are shown for **d**: a transition from cold to temperate ice, and **e**: a mid-glacier apparent temperate ice zone.

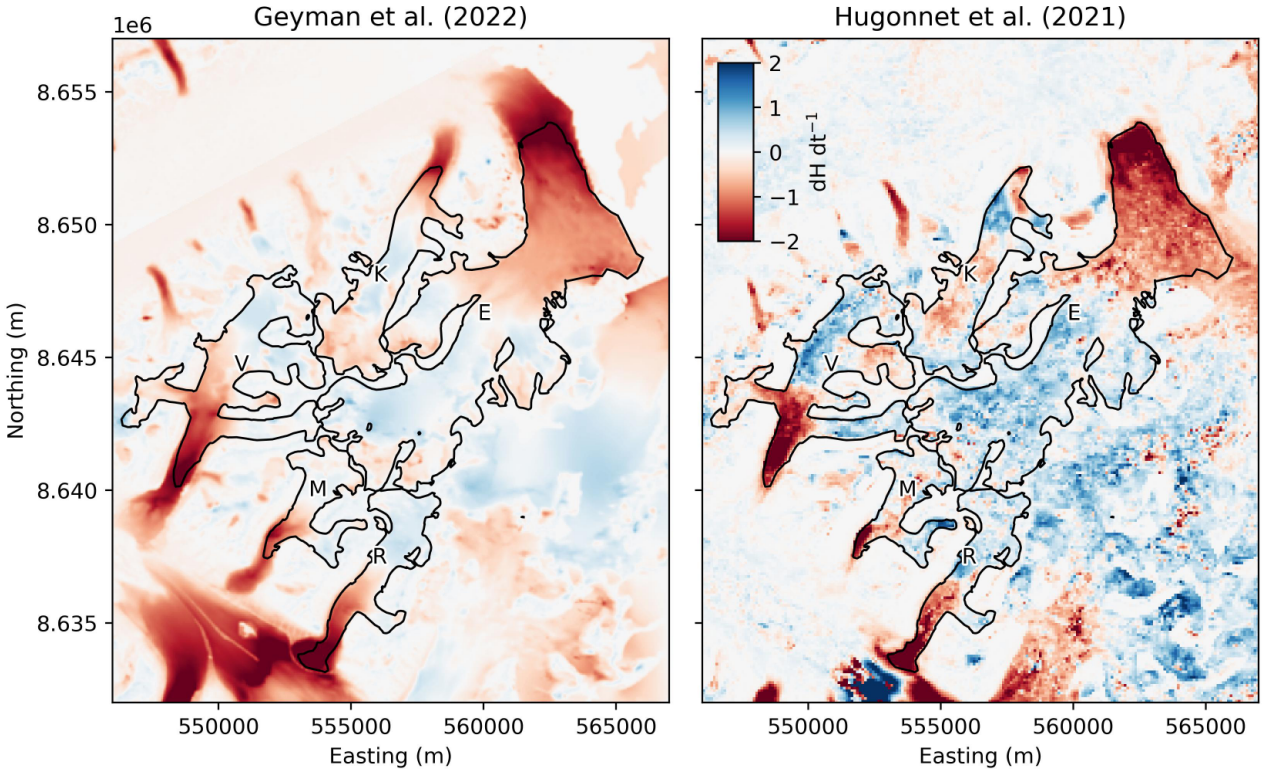

Figure S7. Elevation change rates (dH dt^{-1}) in Heer Land contextualizing the out-of-balance conditions that may be related to abnormal thermal regimes. **Left:** Rates from 1936–2010 (Geyman and others, 2022), and **right:** rates from 2000–2020 (Hugonnet and others, 2021). The glaciers outlined in black are glaciers discussed in this study. They are annotated by the first letter of their names: Vallåkrabreen, Kroppbreen, Edvardbreen, Ragna-Mariebreen, and Mettebreen.